The dissociation mechanism and thermodynamic properties of $HCl_{(aq)}$ in hydrothermal fluids (to 700 °C, 60 kbar) by *ab initio* molecular dynamics simulations

Yuan Mei[1,2*], Weihua Liu[1], Joël Brugger[2], David M Sherman[3], Julian D Gale[4]

1. CSIRO Mineral Resources, Clayton, VIC 3168, Australia
2. School of Earth, Atmosphere and the Environment, Monash University, Clayton, VIC 3800, Australia
3. School of Earth Sciences, University of Bristol, Bristol BS8 1RJ, UK
4. Curtin Institute for Computation/The Institute for Geoscience Research, Curtin University, PO Box U1987, Perth, WA 6845, Australia.

*Corresponding author: yuan.mei@csiro.au

Abstract

HCl is one of the most significant volatiles in the Earth's crust. It is well established that chloride activity and acidity (pH) play important roles in controlling the solubility of metals in aqueous hydrothermal fluids. Thus, quantifying the dissociation of HCl in aqueous solutions over a wide range of temperature and pressure is crucial for the understanding and numerical modeling of element mobility in hydrothermal fluids. Here we conducted *ab initio* molecular dynamics (MD) simulations to investigate the mechanism of $HCl_{(aq)}$ dissociation

and to calculate the thermodynamic properties for the dissociation reaction at 25 to 700 ºC, 1 bar to 60 kbar, i.e. including high temperature and pressure conditions which are geologically meaningful but difficult to investigate via experiments.

Our results predict that $HCl_{(aq)}$ tends to associate with increasing temperature, and dissociate with increasing pressure. In particular, $HCl_{(aq)}$ is highly dissociated at extremely high pressures, even at high temperatures (e.g., 60 kbar, 600-700 ºC). At 25 ºC, the calculated logK_d values (6.81±0.63) are close to the value (7.0) recommended by IUPAC (International Union of Pure and Applied Chemistry) and some previous experimental and theoretical studies (Simonson et al., 1990; Sulpizi and Sprik, 2008, 2010). The MD simulations indicate full dissociation of HCl at low temperature; in contrast, some experiments were interpreted assuming significant association at high HCl concentrations (≥1 m HCl_{tot}) even at room T (logK_d ~0.7; e.g., Ruaya and Seward, 1987; Sretenskaya, 1992; review in Tagirov et al. 1997). This discrepancy is most likely the result of difficulties in experimental determination of minor (if any) concentration of associated $HCl_{(aq)}$ under ambient conditions and thus the activity model used, rather than a reflection of speciation in the solution. With increasing temperature, the discrepancy between our MD results and previous experimental studies, and between different studies, becomes smaller as the degree of HCl association increases. The MD simulations and available experimental studies show consistent results at hydrothermal conditions (300-700 ºC, up to 5 kbar). The new thermodynamic properties based on the MD results provide an independent check of the dissociation constants for $HCl_{(aq)}$, and the first dataset on HCl dissociation in high P-T fluids (up to 60 kbar, 700 ºC) beyond available experimental conditions. Our results will enable prediction of the role of HCl in controlling element mobility in deep earth hydrothermal systems, down to ultra-high pressure metasomatism associated with subduction zone fluids.

1 Introduction

1.1 The dissociation of HCl in geological fluids

Hydrogen chloride (HCl) is one of the most significant volatiles in the Earth's crust. In aqueous solutions, the neutral $HCl_{(aq)}$ ion pair dissociates to the hydrogen ion (H^+) and chloride anion (Cl^-) through a reversible chemical reaction:

$$HCl_{(aq)} \rightleftharpoons H^+ + Cl^- \quad (1)$$

Both H^+ and Cl^- are important in controlling mineral solubility and element mobility in natural and man-made hydrothermal fluids. The chloride anion (Cl^-) is one of the most abundant anions in hydrothermal fluids, and plays an important role in promoting element transport in hydrothermal fluids by forming stable chloro-complexes with many metals (e.g., Cu^+, Co^{2+}, Zn^{2+}, Pb^{2+}, Pd^{2+}, etc.), whereas pH is an essential control of mineral solubility and element speciation in aqueous solutions (as reviewed in Seward and Barnes, 1997; Brugger et al., 2016). Hence, the knowledge of the dissociation mechanism and thermodynamic properties of $HCl_{(aq)}$ over a wide range of temperature and pressure is crucial for the understanding of metal transport and deposition in hydrothermal fluids.

The logarithm of the dissociation constant of $HCl_{(aq)}$ (Eq. 1, $\log K_d$) can be expressed as

$$\log K_d(P,T) = \log a_{H^+} + \log a_{Cl^-} - \log a_{HCl_{(aq)}} \quad (2)$$

where a refers to the activities of the subscripted species. Experiments up to 700 ºC/3.5 kbar, and thermodynamic extrapolations have quantified the dissociation of HCl in aqueous fluids (summarized in Table 1). At low temperature, significant discrepancies up to 6 orders of magnitude exist between the dissociation constants reported by different studies (see Table 1), a result of the different experimental approaches and data interpretation models involved (Simonson et al. 1990). For instance, a few experimental studies obtained the dissociation constant of $HCl_{(aq)}$ by measuring the partial vapor pressure to determine the activity of $HCl_{(aq)}$

70 ($a_{HCl_{(aq)}}$) (e.g., Robinson, 1971; Marsh and McElory, 1985). In these studies, the equilibrium
71 of $HCl_{(aq)} \rightleftharpoons HCl_{(g)}$ was calculated based on Raoult's Law, yielding a value of logK_d ($HCl_{(aq)}$)
72 around 6.2 at 25 ºC. Textbooks (e.g., p. 952 of Greenwood and Earnshaw, 1984) and the
73 IUPAC dataset (p. 46 of Perrin, 1982) list a similar logK_d value of 7. However, Clegg and
74 Brimblecombe (1986) pointed out that the approach based on Raoult's Law is inappropriate
75 for strong acids like HCl, and the Henry's Law constant is a better approach to describe
76 equilibrium between the vapor pressure of HCl solution and dissociated H^+ and Cl^- ions.
77 In contrast, several studies based on potentiometric and conductance data (Table 1) gave
78 values as low as 0.9 (e.g., Johnson and Pytkowiz, 1978; Sretenskaya, 1992), implying
79 significant ion pairing even at room temperature. The extrapolation of Ruaya and Seward
80 (1987)'s $AgCl_{(s)}$ solubility measurements at 100-350 ºC also indicated a logK_d value of 0.7 at
81 room temperature, and Sverjensky et al. (1991) recommended a logK_d value at 0.86 based on
82 a fit of the experimental solubility data for alkali minerals.
83 Different chemical models have been employed to calculate the dissociation constants
84 based on the available experimental data. For example, based on Holmes et al. (1987)'s
85 excess thermodynamic data, Simonson et al. (1990) calculated two sets of the dissociation
86 constants of $HCl_{(aq)}$ using two types of data treatment (as listed in Table 1), and obtained a
87 logK_d at 25 ºC of 7.6 based on the ion association-interaction model (Pitzer's model), and 0.2
88 based on the activity expansion-chemical equilibrium model. The logK_d from different studies
89 generally converge with increasing temperature to mostly overlap at temperatures ≥300 ºC
90 (Tagirov et al., 1997; Sverjensky et al., 1999; Ho et al., 2001). This reflects the increased
91 association of HCl making measurements more achievable. There are still some small
92 discrepancies, in particular between mineral solubility and conductance measurements, and in
93 low-density (<0.6 g cm^{-3}) fluids. For example, there is up to 1 order of magnitude difference

among the logK_d values reported by Franck (1956), Frantz and Marshall (1984) and Sverjensky et al. (1991).

The Helgeson-Kirkham-Flowers (HKF) model has been widely used to fit logK_d($HCl_{(aq)}$) at high temperature (e.g., Sverjensky et al., 1991; Tagirov et al., 1997; Pokrovskii, 1999). The logK_d values extrapolated by the HKF model, based on mineral equilibrium data for K-feldspar-muscovite-quartz (Sverjensky et al., 1991) and AgCl(s) solubility experiments (Tagirov et al., 1997), are within a range of half a log unit at high temperature (300-600 ºC, 0.5-2 kbar).

1.2 pKa measurements via Molecular Dynamics Simulations

Over the past few decades, *ab initio* MD has been playing an increasingly significant role in understanding the molecular structures and thermodynamics of aqueous systems over a wide range of T, P, and solution compositions. In particular, the dissociation of acids at room temperature has been investigated quantitatively using such *ab initio* MD approaches. Trout and Parrinello (1998) first calculated the free energy of H_2O dissociation using *ab initio* distance-constrained thermodynamic integration. Although their results are 16.7 kJ/mol less than the experimental values due to the choice of the density functional and finite size of the system (due to limited computing power at the time), they first demonstrated the capability of quantitative prediction of thermodynamic properties for aqueous species. Later on Sprik (2000) calculated the logK_d of liquid water at ambient conditions using *ab initio* thermodynamic integration based on the coordination number of a given oxygen by hydrogen atoms and obtained values that are within one log unit of the experimental value.

In recent years new techniques have been used to provide a molecular-level understanding of the association of $HCl_{(aq)}$. Chialvo et al. (2002, 2003, 2007) conducted potential of mean force (PMF) calculations based on force-field molecular dynamics simulation to predict the dissociation constants as a function of solution density. They used Lennard-Jones potentials

between the oxygen in rigid H_2O and H_3O^+ molecules and the Cl^- ion to model intermolecular interactions, and obtained reasonable representations of properties such as dielectric constant of water at near critical conditions and the logK_d values as function of density changes. However, those studies did not provide direct association/dissociation constants as a function of temperature and pressure. Murakhtina et al. (2006) used density functional theory (DFT) based *ab initio* MD to calculate the H-NMR chemical shift of $HCl_{(aq)}$, and showed good agreement with experimental results. Sulpizi and Sprik (2008; 2010) applied *ab initio* thermodynamic integration by constraining a dummy proton to calculate the free energy of dissociation of a series of acids ('vertical energy gap' technique); they obtained excellent agreement for logK_d (57 ºC) values to within 0.4 log units for several small acid molecules (HCl, H_2S, formic acid), and within 2 log units for the wide range of acids investigated. They obtained logK_d values of 6.7~7.1 for $HCl_{(aq)}$ at 57 ºC (330 K), in excellent agreement with the IUPAC value of 7 at 25 °C (Perrin, 1982).

Recently *ab initio* MD has also been widely used in molecular-level understanding of the geometry of metal complexes and the energetics of ligand exchange reactions relevant for metal transport in hydrothermal fluids (e.g., Cu(I)–Cl^-, Sherman, 2007; Mei et al., 2014; Au(I)–HS^-, Liu et al., 2011; Cu(I)–HS^-–Cl^-, Mei et al., 2013a; Ag(I)–Cl^-, Liu et al., 2012; Pokrovski et al., 2013; Ag(I)-HS^-/OH^-, He et al., 2016; Au(I)–HS^-/OH^-/S_3^-, Mei et al., 2013b; Pokrovski et al., 2015; Au(I)-Cl^-, Mei et al., 2014). Using distance-constrained thermodynamic integration, our previous studies successfully predicted the quantitative thermodynamic properties for the formation constants for Cu(I)–Cl^-–HS^- (Mei et al., 2013a), Zn(II)–Cl^- (Mei et al., 2015b), Zn(II)-HS^- (Mei et al., 2016) and Pd(II)–Cl^-–HS^- (Mei et al., 2015a). Two studies have successfully measured acid dissociation constants using *ab initio* MD simulations under hydrothermal conditions. Liu et al. (2013) obtained agreement to within 2 pKa units for molybdic acid to 300 ºC, and Liu et al. (2015) obtained agreements of

within 1 unit for pKa_1 of $As(OH)_{3(aq)}$ to 300 ºC, and for $pKa_{1\ to\ 3}$ of $As(HS)_{3(aq)}$ at 25 ºC (no experimental values exist at $T \geq 25$ ˚C).

1.3 Aims of this study

Despite all the experimental and theoretical studies dedicated to HCl association, there is no *ab initio* MD study of $HCl_{(aq)}$ dissociation at elevated temperature, and the mechanism of the increasing ion pairing/association of $HCl_{(aq)}$ with increasing temperatures has not been clarified. There is also no data for HCl dissociation constants at ultra-high P-T relevant to mantle metasomatism and ultra-high pressure subduction environments (up to 60 kbar, 1000 ºC). Under such conditions the role of HCl in controlling pH and metal complexation is unknown.

The present study aims to address these knowledge gaps in order to improve our understanding of the $HCl_{(aq)}$ dissociation/association mechanism, provide an independent check of the dissociation constants, and provide the first dataset for HCl dissociation at ultra-high P-T fluids.

Hence, we conducted *ab initio* molecular dynamics (MD) simulations to investigate the association mechanism of $HCl_{(aq)}$ as a function of temperature and pressure (25–700 ºC, 1 bar to 60 kbar), and then calculated dissociation constants of $HCl_{(aq)}$ based on distance-constraint thermodynamic integration. The dissociation constants obtained from *ab initio* MD simulations were then used to fit thermodynamic properties using the HKF model and DEW model (Sverjensky et al., 2014). These properties allow estimation of the role of HCl in controlling fluid pH and element mobility in deep earth fluids.

Table 1. Review of previous experimental and thermodynamic studies.

2 Methods

2.1 *Ab initio* molecular dynamics simulations

Ab initio MD simulations were performed using the Car-Parrinello molecular dynamics code CPMD (Car and Parrinello, 1985). This method implements density functional theory using plane-wave basis sets and pseudo-potentials for the core electrons and the nucleus. The BLYP exchange-correlation functional was employed with a cutoff for the gradient correction of 5×10^{-8} a.u. (Lee et al., 1988; Becke, 1988). Plane-wave cutoffs of 80 Ry (1088.46 eV) were used together with Martins–Troullier pseudo-potentials generated using the valence electron configuration $3s^2 3p^5$ for Cl (Troullier and Martins, 1991). The BLYP functional provides a good description of water properties such as O–O interaction, angular distributions, coordination numbers and H-bond statistics when compared with neutron diffraction data (Lin et al., 2012), and together with Martins-Troullier pseudo-potentials has been previously employed to study the dissociation mechanism of H_2O molecules in liquid water (Trout and Parrinello, 1998). However, we note that there is a well-known tendency for most functionals, including BLYP, to over-structure liquid water (Lee and Tuckerman, 2006; Lin et al., 2012). Bankura et al. (2014) also showed that BLYP, like most other functionals, best reproduces the properties of water at ambient conditions when using an elevated temperature (80 ºC in their case). It therefore could be argued that there is a temperature offset of approximately 55 ºC between the computed data and experiment in terms of the properties of the solvent. We also note the description of bulk water may be further improved through the inclusion of dispersion corrections, such as for BLYP-D3 (Bankura et al., 2014), though it is unknown whether this would substantially change the results for pKa values. Results from a different GGA functional (DFT-HTCH/120) have been shown to be in good agreement with experiment for the pKa values of several weak organic acids even without further correction for dispersion (Tummanapelli and Vasudevan, 2014).

All *ab initio* MD simulations were performed in the NVT ensemble. Temperatures were controlled by the Nosé thermostat for both ions and electrons. A time-step of 3 a.u. (0.073 fs) was used to stabilize the simulations and a fictitious electron mass of 400 a.u. (3.644×10^{-28} kg) was used to obtain convergence of the energy of the total Car-Parrinello (CP) Hamiltonians.

Ab initio MD simulations of HCl in aqueous fluids were performed at 25–700 ºC from vapor-saturated pressures (P_{sat}) to 60 kbar as listed in Table 2. Each simulation contained 54 H_2O molecules and one HCl in a cubic box with periodic boundary conditions corresponding to bulk HCl concentrations of 1 molal. We set the size of the simulation boxes to correspond to the density of water (0.388 to 1.420 g/cm^3) at the pressure and temperature of interest. Water densities were taken from the equation-of-states contained within the NIST database (Lemmon et al., 2000) at pressures of up to 5 kbar, and from Zhang and Duan (2005) for pressures in the range 10-60 kbar. The densities of the simulation boxes were calculated assuming that they contained 55 H_2O molecules. The initial H-Cl distance was fixed at 1.27 Å, corresponding to the H-Cl distance in the gas-phase HCl molecule (Table 17.11 of Greenwood and Earnshaw, 1984) (Fig. 1). The initial atomic configurations of each simulation were generated by classical MD using the SPC/E potential for water and chloride (Smith and Dang, 1994). Each *ab initio* MD simulation was run for more than 15 ps (>200,000 steps). The radial distribution functions (RDF) for the Cl-H, Cl-H and H-O pairs and their integrals (reflecting the time averaged coordination numbers) were calculated using VMD (Humphrey et al., 1996) to characterize the time averaged structural information.

Table 2. Simulation details

Figure 1. Simulation set up of HCl in aqueous solution

2.2 Thermodynamic integration

The free energies of dissociation of the HCl molecule in aqueous fluids at different temperatures and pressures are crucial for studying the equilibrium formation constants of $HCl_{(aq)}$. We used the thermodynamic integration method introduced by Trout and Parrinello (1998) to calculate the free energy surface for the dissociation of $HCl_{(aq)}$ (Eq. 1) from 25 ºC to 700 ºC, following the procedure used in our previous work (Mei et al., 2013a, 2014, 2015a,b, 2016). Eq 1 can be written as:

$$H^*\text{-}Cl_{(aq)} + H_2O \rightleftharpoons [H_2O\text{-}H^*]^+ + Cl^- \quad (3)$$

where H* is the distance-constrained proton. Distance-constrained MD runs were conducted by fixing H*-Cl distances at certain reaction coordinates, from 1.27 Å to 2.00 Å (Fig. 2). In stage (I), the H*-Cl distance was constrained at 1.27 Å, corresponding to the bond distance of the HCl molecule in isolation. When moving the hydrogen atom away from Cl, one water molecule came close to H*. For example, when H*-Cl was constrained at 1.6 Å (25 ºC), the H*-O distance was 1.14 Å (Fig. 2). In stage (II), at a H*-Cl distance of 2.0 Å, H* associated with one water molecule to form the H_3O^+ ion; the HCl molecule was completely dissociated at this stage. The mean constraint force *f(r)* necessary to maintain the H*-Cl distance was measured at each distance-constraint MD run, sampling possible configurations of H*, Cl and the surrounding solvent. Then the free energy of the dissociation reaction (Eq. 3) was calculated by integrating *f(r)* with respect to the constrained distance (Trout and Parrinello, 1998; Sprik and Giovanni, 1998):

$$\Delta A_{r(I\rightarrow II)} = -\int_I^{II} \langle f(r) \rangle dr \quad (4)$$

Thermodynamic integration calculations were performed at the T-P conditions listed in Table 2. At each temperature, at least ten distance-constrained MD simulations were conducted to obtain the free energy surface. Each simulation was calculated for 8–15 ps, including 1.5 ps for equilibration. In total, more than 2 ns of MD simulations were conducted

in this study to calculate the free energy of HCl dissociation reaction at different temperatures and pressures.

Figure 2. Demonstrating the reaction path and constrained MD

2.3 Calculation of thermodynamic properties

As all the calculations are performed at constant volume, the Helmholtz free energies $\Delta A_{r(I\to II)}$ were obtained. To calculate the formation constant, the Gibbs free energies of the reaction were approximated by neglecting the contribution of pressure change (i.e., $\int_{P_0}^{P} dP = 0$ in Eq. 5):

$$\Delta G_r(P,T) = \Delta A_{r(I\to II)}(V,T) + V\int_{P_0}^{P} dP \qquad (5)$$

where V is the volume of the simulation box.

The standard Gibbs free energies $\Delta G_r^0(P,T)$ for reaction in Eq. 1 can be calculated after activity corrections, as discussed in Mei et al. (2013a, 2015a,b, 2016), according to;

$$\Delta G_r^0(P,T) = \Delta G_r(P,T) + RT\ln\frac{C_{H^+}\gamma_{H^+}\cdot C_{Cl^-}\gamma_{Cl^-}}{C_{HCl_{(aq)}}\gamma_{HCl_{(aq)}}} \qquad (6)$$

where C_i are the concentrations of reactant/products of reaction in Eq. 1, and γ_i are the corresponding activity coefficients. We used the B-dot extension of Debye–Hückel theory (Eq. 7) to estimate the activity coefficients for the individual ions in the solution (Helgeson and Kirkham 1974; Helgeson et al., 1981). Here the logarithm of the activity coefficients are given by;

$$\log\gamma_i = -\frac{z_i^2 A_\gamma I^{1/2}}{1+\mathring{a}_i B_\gamma I^{1/2}} + \dot{B}_\gamma I \qquad (7)$$

where z_i is the charge of the subscripted ion, I is the ionic strength on the molality scale (m), $\mathring{a}_i$ is the ion size parameter in Angstrom ($\mathring{a}_i$ = 4 for Cl^-). A_γ and B_γ are defined in Table 1 and Table 2 in Helgeson and Kirkham (1974). To evaluate the effect of activity coefficients at high pressure, we extended the B-dot parameters assuming that the extended Debye–Hückel equation could be empirically extrapolated to 1000 ºC, 70 kbar using the density of water (Helgeson and Kirkham 1974; Helgeson et al., 1981). The same extrapolation has been employed by Facg et al. (2014) in calculating aqueous ion activity coefficients in the calcium carbonate-water system.

Finally, the dissociation constants ($\log K_d(P,T)$, Eq. 2) were calculated from:

$$\Delta G_r^0(P,T) = -2.303RT\log K(P,T) \quad (8)$$

where R is the gas constant and T is temperature in Kelvin.

Using the Gibbs free energy of the dissociation reaction obtained from thermodynamic integration, we calculated the standard Gibbs energy of formation from the elements for $HCl_{(aq)}$ ($\Delta G^0_{f,HCl_{(aq)}}$) (Table 3). These $\Delta G^0_{f,HCl_{(aq)}}$ values were used to regress the Helgeson–Kirkham–Flowers (HKF) equation-of-state parameters (Helgeson et al., 1981) using the OptimB software (Shvarov, 1999; 2015).

3 Results

3.1 Dissociation as a function of temperature from *ab initio* MD simulations

Unconstrained *ab initio* MD simulations of $HCl_{(aq)}$ were conducted at 25-700 ºC, up to 60 kbar (Table 2) with an initial H-Cl distance of 1.27 Å (Fig. 1). At 25 ºC, 1 bar, the HCl molecule dissociated very early in the simulation (in 0.3 ps), and chloride existed as the free Cl^- ion during the remaining simulation time of 18.86 ps. Fig. 3a shows the time evolution of

283 the H-Cl distance during the first 2 ps of the simulation. From data in the range 100-250 ºC
284 (100 bar), the HCl ion pair was found to last for increasingly longer periods of time with
285 increasing temperature. The HCl molecule first dissociated at times of ~0.5 ps at 100 ºC,
286 ~1.3 ps at 200 ºC, and ~1.5 ps at 250 ºC, while no dissociation was observed at 350 ºC during
287 the whole simulation of 16.62 ps (Fig. 3a).

288 The dynamics of H-Cl distances shown in Fig. 3 provide a qualitative overview of the
289 relative stability of the HCl molecule as a function of temperature. To obtain quantitative
290 information about H-Cl ion pairing, the radial distribution functions (RDF) of Cl-H and Cl-O
291 and their integrals (coordination number, CN) over MD runs of 15-21 ps (see Table 2 for
292 details) were calculated after equilibration for 1.4 ps. As shown in Fig. 4a, at 25 ºC, there is
293 no peak at distances less than 1.6 Å ($CN_{C\text{-}H}$=0), indicating that $HCl_{(aq)}$ was completely
294 dissociated as Cl^- and H^+. The first peak in the Cl-H RDF curve appears at 2.11 Å,
295 corresponding to the distance between the Cl^- ion and the closest H in the water molecule in
296 the hydration shell of the chloride ion, i.e. Cl-H hydrogen-bonding interaction. At 25 ºC, 1 bar,
297 the integral of the Cl-O RDF at 3.8 Å (this Cl-O distance cutoff of RDF plot was chosen
298 according to Mei et al., 2014) gave a coordination number of 5.9 (Table 2), indicating that Cl^-
299 is surrounded by approximately six waters of hydration, which is consistent with previous
300 MD simulation results (Driesner et al., 1998; Sherman 2007, 2010; Mei et al., 2014). The
301 RDF functions of O-O at each temperature show no long-range peaks, indicating the
302 characteristics of liquid water. One snapshot representing six hydration waters in the first
303 shell of Cl^- at 25 ºC is shown in Fig. 5a. The second peak in the Cl-H RDF curve at ~3.51 Å
304 (Fig. 4a) corresponds to the average distance between Cl^- and the further H atoms in the
305 waters of hydration. Similar Cl-H and Cl-O distributions and their integrals show H-Cl
306 dissociation, and ~6 hydration water around Cl^- were obtained from RDF plots of simulations
307 at 100 – 250 ºC, 100 bar (e.g., Fig. 4b; Table 2).

At 300 ºC, 110 bar, the Cl^- ion and the $HCl_{(aq)}$ ion pair was found to be in dynamic equilibrium over the 16 ps simulation time (Fig. 3b). The initial HCl ion pair dissociated within 1 ps, but several other hydrogens combined with chloride to form a bond for short periods of time, resulting in a dynamic exchange between $HCl_{(aq)}$ and Cl^- over the simulation time. Accordingly, in the RDF plot of H-Cl pairs (Fig. 4c) the peak around 1.30 Å reflects $HCl_{(aq)}$ association in solution. The coordination number of 0.36 for this peak suggests that on average during the course of the simulation the $HCl_{(aq)}$ molecule accounted for 36% of chloride in the solution (Table 2), the rest being present as free chloride ion (Cl^-). The second Cl-H RDF peak at around 2.10 Å is broader than at lower temperatures, with a CN value of 4.6, which demonstrates that there are fewer water molecules in the first hydration shell of $HCl_{(aq)}$ as compared to the free Cl^- ion. Figs 5b,c show the co-existence of two chloride species during these simulations; Cl^- with five hydration waters, and $HCl_{(aq)}$ with three hydration waters.

Pressure was found to have a strong effect on the stability of $HCl_{(aq)}$ in our simulations. Increasing pressure at a given temperature causes $HCl_{(aq)}$ to become more dissociated. For example at 300 ºC, 1 kbar, the RDF plot shows only a small peak around 1.3 Å, and the integration of this peak indicates 9% of associated $HCl_{(aq)}$ (Table 2). At 300 ºC, 5 kbar, $HCl_{(aq)}$ completely dissociated to Cl^-. The higher pressure also resulted in a large number of waters of hydration around Cl^-, which is 6.82 according to the RDF calculation (Fig. 4d, Table 2).

At 350 ºC, 200 bar, the $HCl_{(aq)}$ ion pair was the predominant form of chloride during the simulation (94%), while the hydration number of chloride dropped to three. At 400 ºC, 308 bar (Fig. 4e), there is a sharp peak for Cl-H distances around 1.3 Å, with an integral of one, indicating 100% associated $HCl_{(aq)}$ during this simulation. In contrast, $HCl_{(aq)}$ became mostly dissociated at 400 ºC, 5 kbar (Fig. 4f): although a peak of Cl-H pair remains at 1.3 Å, the $CN_{Cl\text{-}H}$ value of 0.1 indicated that only 10% of chloride exists in the form of $HCl_{(aq)}$.

At 500-700 ºC, 1.5-3.5 kbar (density=0.6-0.7 g/cm^3), $HCl_{(aq)}$ remained as the only chloride species in solution. For example, Fig. 4g shows the distribution of Cl-H at 700 ºC, 3.5 kbar. The sharp peak at ~1.3 Å indicates the association between H and Cl, and the integral value of 1 for this peak shows that HCl remains completely associated.

Increasing pressure at 700 ºC resulted in increasing dissociation of $HCl_{(aq)}$. At 10 kbar, $HCl_{(aq)}$ became partially dissociated (63% $HCl_{(aq)}$ and 37% Cl^-), and at 20 kbar only 16% of $HCl_{(aq)}$ ion pairs remained in the solution. At 60 kbar, the MD simulation shows that $HCl_{(aq)}$ was almost completely dissociated (CN_{Cl-H}=0.02; Fig. 4f). The hydration number of chloride (CN_{Cl-O}) also increased with increasing pressure from 3.68 at 3.5 kbar to 11.4 at 60 kbar (Table 2).

Figure 3 Dynamic distance of H-Cl

Figure 4 RDF plots

Figure 5 Snapshots show the first hydration shell of Cl^- and $HCl_{(aq)}$

3.2 Thermodynamic integration and free energy calculation

The results of unconstrained MD simulations described above provide qualitative information about the structural properties (e.g., hydration numbers) and the relative stability of $HCl_{(aq)}/Cl^-$ over the investigated P,T range. The final aim of this study is to calculate the dissociation constants of $HCl_{(aq)}$ in aqueous fluids, and extrapolate these properties to a wide range of T-P conditions. To this end, we performed series of distance-constrained molecular simulations to explore the free energy surface of the $HCl_{(aq)}$ dissociation reaction, as described in Section 2.2. Fig. 6 shows the distance-constrained MD calculations and the constraint mean force collected at each distance at 100 ºC, 100 bar and 400 ºC, 308 bar according to the reaction pathway illustrated in Fig. 2. At 100 ºC, 100 bar, the constraint mean force has a large positive value (145.21 kJ Å^{-1} mol^{-1}) when the H-Cl distance is fixed at 1.27 Å,

indicating a large repulsive force between H and Cl (Fig. 6a). As a result, $HCl_{(aq)}$ tends to dissociate rapidly at 100 ºC, 100 bar (as shown in Fig. 3a). This force becomes smaller at a H-Cl distance of 1.3 Å, and then reaches the minimum value of 1.29 kJ $Å^{-1}$ mol^{-1} at 1.4 Å. At this constraint distance, H-Cl captures one H_2O molecule to form a Cl-H-H_2O structure. However, this structure becomes more stable as the H-Cl distance increases, and a positive force is required to keep H at a constrained distance < 2.1Å, indicating that $HCl_{(aq)}$ spontaneously dissociates at these distances.

We also monitored the distances between the constrained H* (in Eq 3) and nearest O to investigate the association between a proton and a water molecule through the reaction. Fig. 7 shows the H*-O distances as a function of the H*-Cl constraint distances for the reaction at 100 ºC, 100 bar. For the $HCl_{(aq)}$ molecule (stage (I); H*-Cl distance of 1.27 Å), the nearest O neighbors of H* are located at an average H*-O distance of 1.80 Å. When H* moves away from Cl, a water molecule from the solvent gets closer to the H* atom. For example, the H*-O distance is 1.14 Å when $d_{H^*\text{-}Cl}$ = 1.60 Å. The final H*-O distance is 1.0 Å – essentially the same as in a free water molecule (stage II; $d_{H^*\text{-}Cl}$ = 2.0 Å), indicating that $H^*Cl_{(aq)}$ has dissociated fully, and H* has bonded with another O to form H_3O^+ (or formed H_2O and displaced a further H ion to the solvent to form H_3O^+). To get the free energy of the dissociation reaction, the mean constraint force was integrated over the constraint distances from 1.27 Å to 2.00 Å (Eq 4).

At 400 ºC, 308 bar (Fig. 6b), the free energy profile shows a different trend compared to 100 ºC, 100 bar. The large positive value of constraint mean force at 1.27 Å remains, but this force drops significantly with increasing H*-Cl distance, and becomes negative when $d_{H^*\text{-}Cl}$ > 1.3 Å. The large negative force indicates that an external force has to be applied to maintain a given H-Cl distance to balance the attractive force between H^+ and Cl^-, which

agrees with the unconstrained MD results showing that the $HCl_{(aq)}$ molecule is stable in aqueous solutions at 400 ºC, 308 bar (Fig. 4e).

A comparison of free energy surfaces at 25-400 ºC (1-308 bar) reveals two opposite trends for the free energy surfaces below and above 300 °C (Fig. 8a). At 25-250 ºC (1-100 bar), we obtain negative free energy values for the reaction, which indicates that dissociation is favored under those conditions. At 300 ºC, 110 bar, the free energy is close to zero (6.58±1.33 kJ mol^{-1}), in agreement with the unconstrained MD run which shows a dynamic process of association and dissociation (Fig. 3b). At 350 ºC, 200 bar and 400 ºC, 308 bar, the simulations give large positive free energies for the dissociation of HCl, indicating that association is preferred. At 100-400 ºC, for pressures close to the saturation pressure of water, the free energy of the reaction increased systematically as a function of temperature (Fig. 8a).

The effects of pressure on the free energy surfaces of the $HCl_{(aq)}$ dissociation reaction are illustrated in Figs. 8b,c (300 ºC and 400 ºC; P_{sat} (110/308 bar), 1 kbar and 5 kbar). The overall trend is a decrease in free energy with increasing pressure, reflecting increasing dissociation. For example, at 300 ºC, the free energy decreased from +6.58 kJ mol^{-1} at 110 bar to -12.04 kJ mol^{-1} at 1 kbar. In the corresponding MD runs, the proportion of $HCl_{(aq)}$ dropped from 36 to 9% as pressure increased form 110 bar to 1 kbar. At 5 kbar, $HCl_{(aq)}$ dissociated completely, and the free energy became a negative value of -30.28 kJ mol^{-1}. At 400 ºC, $HCl_{(aq)}$ is the predominant species at 308 bar, in agreement with a large positive value of free energy for the dissociation reaction (+48.25 kJ mol^{-1}). At 1 kbar, the free energy value is smaller yet still positive (+9.58 kJ mol^{-1}), reflecting the presence of a small amount of dissociation (3% Cl^-). At 5 kbar, 90% of the chloride exists in the dissociated form, which is reflected by a negative free energy of dissociation (-11.95 kJ mol^{-1}; Fig. 8c).

A similar trend of decrease in the free energy of the dissociation reaction with increasing pressure leading to the predominance of the Cl^- species at $P \geq 1.5$ kbar was observed over the

500-700 ºC temperature range (Fig. 8d). At pressures of 1.5-3.5 kbar (fluid densities 0.6-0.7 g/cm^3), positive free energies were obtained, consistent with the predicted predominance of the $HCl_{(aq)}$ ion pair. At 700 ºC, a free energy of +47.47 kJ mol^{-1} was obtained at 3.5 kbar. At 10 kbar, this free energy value decreases to close to zero (+8.88 kJ mol^{-1}), and then the free energy change decreases with pressure and becomes negative between 20 (-14.89 kJ mol^{-1}) and 60 kbar (-49.72 kJ mol^{-1}). The Gibbs free energies of the $HCl_{(aq)}$ dissociation reaction (Eq. 1) at standard state (ideal 1 m solution) are listed in Table 3. The statistical uncertainty in the free energy of each dissociation reaction was estimated by calculating the standard deviation of the free energy surface at 1.8 – 2.1 Å.

A few sources of uncertainty may affect the reliability of prediction of log*K* values for aqueous complexes using *ab initio* thermodynamic integration (Mei et al., 2013a; 2015a,b; 2016). The convergence of force sampling at low temperature is affected by the kinetics of ions in the solution. Our previous studies of transition metal complexes showed that at T < 300 ºC, the log*K* calculations for Zn(II)-Cl (Mei et al., 2015b) and Cu-Cl-HS (Mei et al., 2013a) complexes gave larger errors than those at T ≥ 300 ºC. Another source of uncertainty is the correction to an infinitely dilute solution and activity coefficients (i.e. the limitations of the B-dot model).

A more complex issue that creates uncertainty lies in defining the free energy difference between $HCl_{(aq)}$ and the separated chloride ion and proton. Firstly, at some conditions there is little or no evidence for a minimum corresponding to the associated stated and so one end state for the reaction in some cases is, at best, a point of inflection in the free energy. Secondly, the limitations of the *ab initio* MD mean that the free energy for the dissociated state corresponds to the hydronium-chloride ion pair. Consequently there should be a further, though smaller, contribution due to the separation of this ion pair to the solvent-shared,

solvent separated ion pairs and beyond. A third and final issue is that through using the Cl-H distance as a constraint, as opposed to the Cl coordination number by hydrogen, there is the possibility that an unconstrained hydrogen ion from another water may ultimately protonate the chloride ion. However, it appears that this is not a problem for short constrained distances since the presence of the adjacent (nascent) hydronium ion is sufficient to disfavor this. Despite these caveats, it appears that good agreement with experimental data is obtained, where available, through using the free energy difference between the system at the HCl bond length and at 2.0 Å as a proxy for the free energy of dissociation.

Figure 6. Examples of free energy calculations at 100 ºC, 100 bar and 400 ºC, 308 bar.

Figure 7. H*-O distances during the thermodynamic integration at 100 ºC, 100 bar.

Figure 8. Free energy surfaces at 25 – 700 ºC.

Table 3. List of Gibbs free energy and logK_d values

3.3 Thermodynamic properties

We fitted the dissociation constant of $HCl_{(aq)}$ (logK_d) calculated from MD simulations at 25-700 ºC, 1-5 kbar to the revised HKF equations (Helgeson et al., 1987; Sverjenky et al., 1997) using the OptimB software (Shvarov, 1999; 2015) to provide a convenient parameterization for the temperature dependence of the dissociation constant. As discussed above, depending on the model used to interpret the room-temperature experiments for HCl association, logK_d of ~0.7 or ~7 are obtained (Table 1). For the current fit, we chose to represent the physical aspect of HCl association, i.e. full dissociation at room temperature even in concentrated HCl solutions (log$K_{d(25\,^{\circ}C)}$ ~ 7). We attempted to include the experimental data at high P-T (up to 5 kbar) into the fit, but this resulted in an unrealistic extrapolation to ultra-high pressure (~20-60 kbar), which did not agree (by several log units) with the MD results at these P-T conditions. Therefore, we opted to use mainly the MD

results in the HKF fitting so that we can provide an independent and an internally consistent dataset for crosschecking of the experimental results, and provide $HCl_{(aq)}$ properties at ultra-high pressure conditions.

As our calculations gave a logK_d value of 6.81 at 25 ºC, 1 bar, the $\Delta_f \overline{G}^0_{P_r,T_r}$ value for $HCl_{(aq)}$ was fixed accordingly at -22,091 cal mol^{-1}. To reduce the number of independent parameters in the fits, the empirical relations for $Cp=f(c_1,c_2)$ and $V=f(a_1, a_2, a_3, a_4)$ were applied (Shock and Helgeson, 1988; Sverjensky et al., 1997; Shvarov, 2015). We choose a $C_{p(298)}$ value of 35.74 cal K^{-1} mol^{-1} and a $V^0_{(298)}$ value of 16.38 cm^3 mol^{-1}, following the review of experimental data by Tagirov et al. (1997). Other proposed $C_{p(298)}$ values for HCl(aq) (e.g., 29 cal K^{-1} mol^{-1} from Sverjensky et al. (1991); and 39 cal K^{-1} mol^{-1} from Pokrovskii (1999)) were also tested in the fitting but the results are similar, therefore Tagirov's value was used as it is close to the average of the three $C_{p(298)}$ values. The $V^0_{(298)}$ values of 16.38 cm^3 mol^{-1} for $HCl_{(aq)}$ listed in Tagirov et al. (1997)'s study is very close to the $V^0_{(298)}$ values of Cl^- (17.79 cm^3 mol^{-1}, Shock et al, 1997) and $HCl_{(aq)}$ (19.0 cm^3 mol^{-1}, Sharygin and Wood, 1997), which makes sense as our MD results also show that the difference of $V^0_{(298)}$ between Cl^- and $HCl_{(aq)}$ is very small based on the change in the effective radius of the solvent sphere of the two species obtained from the Cl-O RDF plot. We also tested the $V^0_{(298)}$ values in the fitting using 16.38, 17.79 and 19.0 cm^3 mol^{-1}, and the results were very similar.

The fitted parameters of the HKF model are listed in Table 4, and the logarithm of the dissociation constants of $HCl_{(aq)}$ at 25-700 ºC, P_{sat}-5000 bar calculated using HCh (Shvarov and Bastrakov, 1999; Shvarov, 2008) based on out fitted HKF parameters are listed in Table 5. Using these HKF parameters, we have calculated the logK_d at 300-1000 ºC, 10-70 kbar listed in Table 6 using the DEW model (Sverjensky et al., 2014). These logK_d values from fitting of HKF parameters and DEW model are in good agreement (within one log unit) with the logK_d values directly calculated from MD simulations (Table 3), suggesting that the properties listed

in Table 6 can be used to assess the stability of $HCl_{(aq)}$ to ultra-high pressures and temperatures (up to 1000 ºC, 70 kbar, Table 6).

Table 4. HKF parameters

Table 5. LogK_d of $HCl_{(aq)}$ at 25 – 700 ºC, Psat – 5 kbar from HKF parameters using HCh

Table 6. LogK_d of $HCl_{(aq)}$ at 700 – 1000 ºC, 10k – 70 kbar from HKF parameters using DEW model.

4 Discussion

4.1 Dissociation and hydration of HCl in aqueous fluids as a function of temperature and pressure

The *ab initio* MD simulations conducted in this study revealed the dissociation/association of $HCl_{(aq)}$ in aqueous fluids over a wide range of temperatures and pressures. At temperatures < 300 ºC and $P \geq P_{sat}$, the $HCl_{(aq)}$ ion pair was unstable and dissociated quickly into H^+ and Cl^-. At temperatures ≥ 300 ºC, the simulations reveal the strong pressure dependence of the association/dissociation of chloride. Upon an increase in pressure from P_{sat} to 5 kbar, the predominant form of chloride changed from associated $HCl_{(aq)}$ to dissociated Cl^-.

The free Cl^- ion at low temperature is stabilized by its hydration shell. At 25 ºC, $HCl_{(aq)}$ completely dissociated to H^+ and Cl^-, and the Cl^- ion is surrounded by six water molecules via hydrogen-bonding to water H atoms (Fig. 5a). The water-water interaction and the interaction between Cl^- and H_2O become weaker with increasing temperature (Driesner et al., 1998; Sherman 2007, 2010). The intensity of the first Cl-H and Cl-O RDF peak decreases with increasing temperature from 25 ºC to 250 ºC, and the integral of this peak becomes smaller, reflecting the decrease in hydration number of Cl^- (Fig. 9). At temperatures above

300 ºC, when the H^+ and Cl^- become associated (e.g., Figs. 4e,g), the interaction between Cl^- and solvent water is much weaker. Based on the evidence from Cl^--H_2O interaction, we can hypothesize that at low temperature, the hydrated Cl^- ion was coordinated by a few water molecules in the first hydration shell (e.g., 6 H_2O at 25 ºC) via Cl-H bonding to stabilize the ion. At high temperature, because the bonding between Cl^- and water H-atoms becomes weaker, the hydration shell is more disordered and not sufficient to stabilize the Cl^- ion. Thus the Cl^- ion tends to associate with a cation, such as $HCl_{(aq)}$ in acidic solutions, or $NaCl_{(aq)}$ in Na^+-bearing brines (Driesner et al., 1998; Mei et al., 2014). Increasing pressure similarly increases the hydration number (e.g., simulations at 300 ºC, 5 kbar and 700 ºC, 60 kbar), which leads to the dissociation of HCl at high pressure.

According to the traditional Born model, the decrease in dielectric constant of the solvent with decreasing solution density at high temperature will cause ion association (Born 1927; Seward and Barnes, 1997). A recent study of the dielectric constant of water also showed the same trend at very high temperature (2000 K) and pressures (110 kbar) (Pan et al., 2013). Our simulations predict increased $HCl_{(aq)}$ association with increasing temperature and decreasing pressure (with decreasing dielectric constant) and predict an increasing fraction of charged species (e.g., Cl^-) at low temperature, high pressure and conversely neutral species (e.g., $HCl_{(aq)}$, $NaCl_{(aq)}$) at high temperature, low pressure. The change of dissociation of $HCl_{(aq)}$ is consistent with the effect of pressure on the change of water properties, such as density and dielectric constant.

An alternative explanation of the increased association HCl at increasing temperatures is the change of entropy. If the hydration shell of chloride is considered, the $HCl_{(aq)}$ dissociation reaction (Eq. 1) can be written as

$$HCl(H_2O)_m + (n\text{-}m+1)H_2O \rightleftharpoons H_3O^+ + [Cl(H_2O)_n]^- \qquad (n\text{-}m\geq 2) \qquad (8)$$

As shown in Fig. 9b, the hydration of chloride also changed as a function of temperature. When chloride exists as free ion, there are 5-7 (n in Eq 8) water molecules surrounding Cl^- (Table 2); in contrast, when $HCl_{(aq)}$ predominates, the hydration number of chloride (m in Eq 8) drops to ~ 1.7-4 (Table 2). Therefore when temperature increases, the change in translational entropy resulting from the HCl association also increases since more water molecules are released from the hydration shell of the Cl^- ion. Indeed our estimated standard entropy change of $HCl_{(aq)}$ association, based on the Van't Hoff relationship (Galaon and David, 2011), increases with increasing temperature and decreases with increasing pressure (Fig. 10). This is consistent with the complexation behavior of aqueous Cu(I)/Au(I)/Zn(II) complexes as discussed by Mei et al. (2014; 2015b) and calcium carbonate ion association studied by Kellermeier et al. (2016); the increase in translational entropy of solvent molecules is the driving force for increased ion pairing with temperature. However, with increasing pressure, the hydration of both $HCl_{(aq)}$ and Cl^- increases. This has the effect of decreasing the entropy change associated with the HCl association, hence contributing to favoring dissociation with increasing pressure. Moreover, the translational entropy of any species will decrease with increasing solvent density.

Figure 9. RDF and CN of Cl-H (a) and Cl-O (b) at different temperature

Figure 10. Change of entropy for $HCl_{(aq)}$ association reaction at different T-P

4.2 Dissociation constants for $HCl_{(aq)}$, compared to previous studies

Selected datasets for the $\log K_d$ of $HCl_{(aq)}$ at elevated temperatures and water-saturated pressure from different studies are compared in Fig. 11. For the 25-350 °C range (Fig. 11a), as summarized in the introduction and in Table 1, there are two different trends depending of the model chosen for data reduction. Ruaya and Seward (1987), Sretenskaya (1992) and Tagirov et al. (1997) recommend a value of ~1 at 25 ºC, implying that small amounts of HCl

552 association exist even at room temperature in concentrated HCl solutions, which is surprising
553 for a strong acid such as HCl. In contrast, Pokrovskii (1999)'s geochemical modeling and
554 Simonson (1990)'s associated ion (AI) model gave logK_d values close to 7 at 25 ºC, which
555 implies full dissociation of HCl. As pointed out by Simonson et al. (1990), any attempt to
556 measure the association constant of $HCl_{(aq)}$ is ambiguous because the degree of association is
557 so small at room temperature. Consequently, the activity of $HCl_{(aq)}$ is too low to be measured
558 reliably by experimental approaches. The logK_d for $HCl_{(aq)}$ derived from solubility results
559 ($AgCl_{(s)}$ and alkali mineral buffers) depend upon the reliability of the thermodynamic data for
560 the solid species and key aqueous species such as Ag-Cl complexes at relatively high ionic
561 strength (>1), and hence the results are highly dependent on the choice of activity coefficient
562 model chosen for the data regression.

563 *Ab initio* MD clearly demonstrates the full dissociation of HCl at room temperature, and
564 validates a logK_d(25 ºC) ~ 7 as the physically correct value. A similar result was obtained in
565 the earlier *ab initio* MD calculations by Sulpizi and Sprik (2008; 2010), who obtained
566 logK_d(57 ºC) very close to 7, the value recommended in the IUPAC database (Perrin, 1982).
567 Sulpizi and Sprik (2010) also show that for several inorganic acids, the predictions based on
568 *ab initio* MD simulations are better than 1.5 logK unit. Our calculations also delivered a value
569 of 6.81±0.63, close to 7. We also note that the lack of HCl association in the 1 m HCl solution
570 studied is highlighted qualitatively in the MD runs; these runs were started from an $HCl_{(aq)}$ ion
571 pair, which quickly dissociated at room-temperature, never to reform.

572 Under hydrothermal conditions, the values derived from MD in this study are generally
573 systematically higher (up to ~1 log unit) than the other models in the temperature range of
574 100-250 ºC (100 bar), indicating that the MD study predicts more dissociation of $HCl_{(aq)}$ than
575 experimental studies in this temperature range. This is probably because 1) it is difficult to

determine the thermodynamic properties for fully dissociated acid with experimental methods as discussed below, 2) limitations to the accuracy of the MD methods discussed in the previous section. Note that because the simulations were started with the $HCl_{(aq)}$ molecule, the slow kinetics at low temperature may cause uncertainty in the HCl dissociation constants due to the timescale for hydrogen-bond network reorganization being comparable to that of the simulation length.

In order to illustrate the differences in predicted solubility arising from using $\log K_d$(HCl) from the different HKF extrapolations, we have recalculated the solubility data at 100-350 ºC of Ruaya and Seward (1987). Since the work of Ruaya and Seward (1987), the stability of Ag(I) chloride complexes and the dissociation constant of $AgCl_{(s)}$ have been revisited by Pokrovski et al. (2013), and these values were used in our calculations. The value for the solubility constant of $AgCl_{(s)}$ was adjusted from -5.99 to -6.1 at 350 ºC, to account for higher than measured solubilities. The results are shown in Fig. 12 and clearly show that all three HKF datasets (Tagirov et al., 1997; Pokrovskii, 1999 and this study) can reproduce the measured solubility reasonably well, with Tagirov's values giving slightly better agreement with the experimental data. Therefore we recommend using the HKF parameters of Tagirov et al. (1997) (Fig. 11a) for the temperature range from 25-300 °C for calculating mineral solubility. HCl is mostly dissociated below 200 ºC (Fig. 12a',b'). However using the experimental dissociation values at 25 ºC (e.g., $\log K_d = 0.9$ from Sretenskaya, 1992), the calculated $HCl_{(aq)}$ is ~6% of total moles of HCl in a 1 molal HCl solution. Therefore for models where the physical amount of HCl association is important (e.g., kinetics, catalysis), HKF parameters that predict full dissociation at room T are more appropriate.

From 350 ºC onwards and pressure up to 5 kbar, most available experimental studies are within a small error range with the MD results (up to one log unit) (Fig. 11b,c). As we

discussed before, *ab initio* MD results become more reliable at high temperature due to the faster kinetics. In addition, the association of $HCl_{(aq)}$ is much stronger than at lower temperature and a more measurable entity; thus the results from various studies are more reliable and less model-dependent. In this temperature range there is no significant difference among the HCl speciation calculated using the HKF models of Tagirov (1997), Pokrovskii (1999) or this study (Fig. 12d'). For example, the three datasets give similar agreements to the AgCl(s) solubilities measured by Rayua and Seward (1987) at 350 ºC (Fig. 12d).

At ultra-high P-T conditions (5-70 kbar) where there is no experimental data available, we recommend the HKF parameters from this study to model HCl speciation. These parameters, when plugged into the DEW model (Sverjensky et al., 2014), produce logK_d values that are in good agreement with the three MD simulated logK_d values at 20, 50 and 60 kbar (Fig. 13), even if these three data points were not included in the HKF-DEW model regressions.

Figure 11. LogK_d comparing with experiments

Figure 12. Solubility of AgCl (Ruaya and Seward, 1987) and calculated values using Tagirov 1997; Prokvskii, 1999 and this study for $HCl_{(aq)}$.

Figure 13. LogK_d extrapolated using HKF parameters at 25-700ºC, Psat-5 kbar, and high pressure (10-60kbar).

5 Conclusion and geological implications

The MD simulations in this study provide insights into the molecular structure and dissociation mechanism of the $HCl_{(aq)}$ molecule and the corresponding products. Despite the uncertainties and limitations of the MD simulation approach, our results provide a reasonable prediction of the dissociation constants for $HCl_{(aq)}$ compared with the existing experimental

623 data. Furthermore, the MD simulations provide the first thermodynamic data for HCl
624 speciation at high pressures relevant to conditions such as for subduction-zone fluids.

625 In recent years, the role of slab-generated aqueous fluids in mantle metasomatism has
626 received much attention for its potential in controlling the mantle oxidation state, metal
627 fertility in arc systems (e.g., Evans and Tomkins, 2011; Galvez et al., 2016). The importance
628 of pH in ultra-high pressure subduction environments was emphasized by Sverjensky and
629 Huang (2015), who proposed that pH changes can drive diamond formation in the presence of
630 aqueous fluids containing organic carbon (900 ºC, 50 kbar). Coincidentally, the highly
631 dissociated $HCl_{(aq)}$ at extreme high pressure in our simulations also suggests that more protons
632 can be released to make the fluids more acidic even at the high temperatures characteristic of
633 ultra-high pressure environments. The dissociation of $HCl_{(aq)}$ at high pressure suggests that in
634 these environments the fluids may rather be acidic, explaining their capacity to dissolve and
635 enrich metals and to react with host mantle rocks. The effect of pressure on the dissociation of
636 $HCl_{(aq)}$ also implies that even at the temperatures of the upper mantle in subduction zones
637 (Manning, 2004), fluids will still have free Cl^- available to complex metals and hence
638 increase their solubility. For the same reason that pressure causes $HCl_{(aq)}$ to dissociate,
639 pressure will decrease the entropy change associated with complexation; this favors
640 dissociation, though this is a second-order effect. The first-order effect of pressure will
641 depend on the molar volume change of the complexation reaction. We have demonstrated that
642 *ab initio* MD simulations using density functional theory employing GGA exchange-
643 correlation functionals can yield reasonable stability constants for aqueous species. The
644 further addition of dispersion corrections and even the use of hybrid functionals in the future
645 will only further improve such simulations. We anticipate that a quantitative thermodynamic
646 model of metal complexation at upper mantle pressures will soon be possible from such
647 simulations.

6 Acknowledgement

Research funding was provided by the CSIRO OCE fellowship to Y.M., and by the Australian Research Council (ARC) to W.L. (FT130100510), J.B. (DP130100471) and J.G. (DP160100677). The MD calculations in this work were supported by resources provided by the Pawsey Supercomputing Centre with funding from the Australian Government and the Government of Western Australia and the high performance computers in CSIRO.

References

Bankura, A., Karmakar, A., Carnevale, V., Chandra, A. and Klein, M.L. (2014) Structure, Dynamics, and Spectral Diffusion of Water from First-Principles Molecular Dynamics. The Journal of Physical Chemistry C 118, 29401-29411.

Becke, A.D. (1988) Density-functional exchange-energy approximation with correct asymptotic behavior. Physical review. A, General physics 38, 3098-3100.

Born, M. and Oppenheimer, R. (1927) Zur quantentheorie der molekeln. Annalen der Physik 389, 457-484.

Brugger, J., Liu, W., Etschmann, B., Mei, Y., Sherman, D.M. and Testemale, D. (2016) A review of the coordination chemistry of hydrothermal systems, or do coordination changes make ore deposits? Chemical Geology 447, 219-253.

Car, R. and Parrinello, M. (1985) Unified approach for molecular dynamics and density-functional theory. Phys Rev Lett 55, 2471-2474.

Chialvo, A.A., Cummings, P.T. and Simonson, J.M. (2003) H_3O^+/Cl^- ion pairing in hydrothermal solutions by simulation and electrical conductance. A review. Journal of Molecular Liquids 103-104, 235-248.

Chialvo, A.A., Ho, P.C., Palmer, D.A., Gruszkiewicz, M.S., Cummings, P.T. and Simonson, J.M. (2002) H_3O^+/Cl^- Association in High-Temperature Aqueous Solutions over a Wide Range of State Conditions. A direct comparison between simulation and electrical conductance experiment. The Journal of Physical Chemistry B 106, 2041-2046.

Chialvo, A.A. and Simonson, J.M. (2007) H_3O^+Cl-Pair Association in Steam and Highly Compressible Aqueous Environments. The Journal of Physical Chemistry C 111, 15569-15574.

Clegg, S.L. and Brimblecombe, P. (1986) The dissociation constant and henry's law constant of HCl in aqueous solution. Atmospheric Environment 20, 2483-2485.

Driesner, T., Seward, T.M. and Tironi, I.G. (1998) Molecular dynamics simulation study of ionic hydration and ion association in dilute and 1 molal aqueous sodium chloride solutions from ambient to supercritical conditions. Geochimica et Cosmochimica Acta 62, 3095-3107.

Evans, K.A., and Tomkins, A.G. (2011) The relationship between subduction zone redox budget and arc magma fertility. Earth and Planetary Science Letters, 308(3-4), 401-409.

Facq, S., Daniel, I., Montagnac, G., Cardon, H. and Sverjensky, D.A. (2014) In situ Raman study and thermodynamic model of aqueous carbonate speciation in equilibrium with aragonite under subduction zone conditions. Geochimica et Cosmochimica Acta 132, 375-390.

Franck, E. (1956) Highly compressed steam. III. Ion dissociation of hydrochloric acid, potassium hydroxide, and water in water above the critical point. Zeitschrift für physikalische Chemie 8, 192-206.

Frantz, J.D. and Marshall, W.L. (1984) Electrical conductances and ionization constants of salts, acids, and bases in supercritical aqueous fluids; I, Hydrochloric acid from 100 degrees to 700 ˚C and at pressures to 4000 bars. American Journal of Science 284, 651-667.

Galaon, T. and David, V. (2011) Deviation from van't Hoff dependence in RP-LC induced by tautomeric interconversion observed for four compounds. Journal of Separation Science 34, 1423-1428.

Galvez, M.E., Connolly, J.A.D. and Manning, C.E. (2016) Implications for metal and volatile cycles from the pH of subduction zone fluids. Nature 539, 420-424.

Greenwood, N.N. and Earnshaw, A. (1984) Chemistry of the elements, 1st ed. Oxford [Oxfordshire]; Pergamon Press, New York.

He, M., Liu, X., Lu, X., Zhang, C. and Wang, R. (2016) Structures and Acidity Constants of Silver–Sulfide Complexes in Hydrothermal Fluids: A First-Principles Molecular Dynamics Study. The Journal of Physical Chemistry A 120, 8435-8443.

Helgeson, H.C. and Kirkham, D.H. (1974) Theoretical prediction of the thermodynamic behavior of aqueous electrolytes at high pressures and temperatures; II, Debye-Huckel parameters for activity coefficients and relative partial molal properties. American Journal of Science 274, 1199-1261.

Helgeson, H.C., Kirkham, D.H. and Flowers, G.C. (1981) Theoretical prediction of the thermodynamic behavior of aqueous electrolytes by high pressures and temperatures; IV, Calculation of activity coefficients, osmotic coefficients, and apparent molal and standard and relative partial molal properties to 600 ˚C and 5kb. American Journal of Science 281, 1249-1516.

Ho, P.C., Palmer, D.A. and Gruszkiewicz, M.S. (2001) Conductivity measurements of dilute aqueous HCl solutions to high temperatures and pressures using a flow-through cell. The Journal of Physical Chemistry B 105, 1260-1266.

Holmes, H.F., Busey, R.H., Simonson, J.M., Mesmer, R.E., Archer, D.G. and Wood, R.H. (1987) The enthalpy of dilution of HCl(aq) to 648 K and 40 MPa thermodynamic properties. The Journal of Chemical Thermodynamics 19, 863-890.

Humphrey, W., Dalke, A. and Schulten, K. (1996) VMD: visual molecular dynamics. J Mol Graph 14, 33-38, 27-38.

Johnson, K.S. and Pytkowicz, R.M. (1978) Ion association of Cl^- with H^+, Na^+, K^+, Ca^{2+}, and Mg^{2+} in aqueous solutions at 25 ºC. American Journal of Science 278, 1428-1447.

Kellermeier, M., Raiteri, P., Berg, J.K., Kempter, A., Gale, J.D. and Gebauer, D. (2016) Entropy Drives Calcium Carbonate Ion Association. ChemPhysChem 17, 3535-3541.

Lee, C., Yang, W. and Parr, R.G. (1988) Development of the Colle-Salvetti correlation-energy formula into a functional of the electron density. Physical Review B 37, 785-789.

Lee, H.-S. and Tuckerman, M.E. (2006) Structure of liquid water at ambient temperature from ab initio molecular dynamics performed in the complete basis set limit. The Journal of Chemical Physics 125, 154507.

Lemmon, E.W., Jacobsen, R.T., Penoncello, S.G. and Friend, D.G. (2000) Thermodynamic properties of air and mixtures of nitrogen, argon, and oxygen from 60 to 2000 K at pressures to 2000 MPa. Journal of physical and chemical reference data 29, 331-385

Lin, I.C., Seitsonen, A.P., Tavernelli, I. and Rothlisberger, U. (2012) Structure and Dynamics of Liquid Water from ab Initio Molecular Dynamics-Comparison of BLYP, PBE, and revPBE Density Functionals with and without van der Waals Corrections. J Chem Theory Comput 8, 3902-3910.

Liu, X., Lu, X., Wang, R., Zhou, H. and Xu, S. (2011) Speciation of gold in hydrosulphide-rich ore-forming fluids: Insights from first-principles molecular dynamics simulations. Geochimica et Cosmochimica Acta 75, 185-194.

Liu, X., Lu, X., Wang, R. and Zhou, H. (2012) Silver speciation in chloride-containing hydrothermal solutions from first principles molecular dynamics simulations. Chemical Geology 294–295, 103-112.

Liu, X., Cheng, J., Sprik, M. and Lu, X. (2013) Solution Structures and Acidity Constants of Molybdic Acid. The Journal of Physical Chemistry Letters 4, 2926-2930.

Liu, X., He, M., Lu, X. and Wang, R. (2015) Structures and acidity constants of arsenite and thioarsenite species in hydrothermal solutions. Chemical Geology 411, 192-199.

Manning, C.E. (2004) The chemistry of subduction-zone fluids. Earth and Planetary Science Letters 223, 1-16.

Marsh, A.R.W. and McElroy, W.J. (1985) The dissociation constant and Henry's law constant of HCl in aqueous solution. Atmospheric Environment (1967) 19, 1075-1080.

Mei, Y., Etschmann, B., Liu, W., Sherman, D.M., Barnes, S.J., Fiorentini, M.L., Seward, T.M., Testemale, D. and Brugger, J. (2015a) Palladium complexation in chloride- and bisulfide-rich fluids: Insights from ab initio molecular dynamics simulations and X-ray absorption spectroscopy. Geochimica et Cosmochimica Acta 161, 128-145.

Mei, Y., Etschmann, B., Liu, W., Sherman, D.M., Testemale, D. and Brugger, J. (2016) Speciation and thermodynamic properties of zinc in sulfur-rich hydrothermal fluids: Insights from ab initio molecular dynamics simulations and X-ray absorption spectroscopy. Geochimica et Cosmochimica Acta 179, 32-52.

Mei, Y., Liu, W., Sherman, D.M. and Brugger, J. (2014) Metal complexation and ion hydration in low density hydrothermal fluids: Ab initio molecular dynamics simulation of Cu(I) and Au(I) in chloride solutions (25–1000 °C, 1–5000 bar). Geochimica et Cosmochimica Acta 131, 196-212.

Mei, Y., Sherman, D.M., Liu, W. and Brugger, J. (2013a) Ab initio molecular dynamics simulation and free energy exploration of copper(I) complexation by chloride and bisulfide in hydrothermal fluids. Geochimica et Cosmochimica Acta 102, 45-64.

Mei, Y., Sherman, D.M., Liu, W. and Brugger, J. (2013b) Complexation of gold in S_3^--rich hydrothermal fluids: Evidence from ab-initio molecular dynamics simulations. Chemical Geology 347, 34-42.

Mei, Y., Sherman, D.M., Liu, W., Etschmann, B., Testemale, D. and Brugger, J. (2015b) Zinc complexation in chloride-rich hydrothermal fluids (25–600°C): A thermodynamic model derived from ab initio molecular dynamics. Geochimica et Cosmochimica Acta 150, 265-284.

Murakhtina, T., Heuft, J., Meijer, E.J. and Sebastiani, D. (2006) First principles and experimental 1H NMR signatures of solvated ions: The case of HCl(aq). Chemphyschem 7, 2578-2584.

Pan, D., Spanu, L., Harrison, B., Sverjensky, D.A. and Galli, G. (2013) Dielectric properties of water under extreme conditions and transport of carbonates in the deep Earth. Proceedings of the National Academy of Sciences of the United States of America 110, 6646-6650.

Pearson, D., Copeland, C.S. and Benson, S.W. (1963) The Electrical Conductance of Aqueous Hydrochloric Acid in the Range 300 to 383°. Journal of the American Chemical Society 85, 1047-1049.

Perrin, D.D. (1982) Table, Ionisation Constants of Inorganic Acids and Bases in Aqueous Solution (Second Edition). Pergamon, pp. 1-138.

Pitzer, K.S. (1973) Thermodynamics of electrolytes. I. Theoretical basis and general equations. The Journal of Physical Chemistry 77, 268-277.

Pokrovskii, V.A. (1999) Calculation of the standard partial molal thermodynamic properties and dissociation constants of aqueous HCl^0 and HBr^0 at temperatures to 1000°C and pressures to 5 kbar. Geochimica et Cosmochimica Acta 63, 1107-1115.

Pokrovski, G.S., Kokh, M.A., Guillaume, D., Borisova, A.Y., Gisquet, P., Hazemann, J.-L., Lahera, E., Del Net, W., Proux, O., Testemale, D., Haigis, V., Jonchière, R., Seitsonen, A.P., Ferlat, G., Vuilleumier, R., Saitta, A.M., Boiron, M.-C. and Dubessy, J. (2015) Sulfur radical species form gold deposits on Earth. Proceedings of the National Academy of Sciences 112, 13484-13489.

Pokrovski G. S., Roux J., Ferlat G., Jonchiere R., Seitsonen A. P., Vuilleumier R. and Hazemann J.-L. (2013) Silver in geological fluids from in situ X-ray absorption spectroscopy and first- principles molecular dynamics. Geochim. Cosmochim. Acta 106, 501–523.

Robinson, R.A. and Bates, R.G. (1971) Dissociation constant of hydrochloric acid from partial vapor pressures over hydrogen chloride-lithium chloride solutions. Analytical Chemistry 43, 969-970.

Ruaya, J.R. and Seward, T.M. (1987) The ion-pair constant and other thermodynamic properties of HCl up to 350°C. Geochimica et Cosmochimica Acta 51, 121-130.

Seward, T.M. and Barnes, H.L. (1997) Metal transport by hydrothermal ore fluids, in: Barnes, H.L. (Ed.), Geochemistry of Hydrothermal Ore Deposits, 3rd Edition ed. Wiley, New York, pp. 435-486.

Sharygin, A.V. and Wood, R.H. (1997) Volumes and heat capacities of aqueous solutions of hydrochloric acid at temperatures from 298.15 K to 623 K and pressures to 28 MPa. The Journal of Chemical Thermodynamics 29, 125-148.

Sherman, D.M. (2007) Complexation of Cu^+ in Hydrothermal NaCl Brines: Ab initio molecular dynamics and energetics. Geochimica et Cosmochimica Acta 71, 714-722.

Sherman, D.M. (2010) Metal complexation and ion association in hydrothermal fluids: insights from quantum chemistry and molecular dynamics. Geofluids 10, 41-57.

Shock, E.L. and Helgeson, H.C. (1988) Calculation of the thermodynamic and transport properties of aqueous species at high pressures and temperatures: Correlation algorithms for ionic species and equation of state predictions to 5 kb and 1000ºC. Geochimica et Cosmochimica Acta 52, 2009-2036.

Shvarov, Y.V. (2008) HCh: New potentialities for the thermodynamic simulation of geochemical systems offered by windows. Geochemistry International 46, 834-839.

Shvarov, Y.V. and Bastrakov, E. (1999) HCh: a software package for geochemical equilibrium modelling. User's Guide Record/25 (Australian Geological Survey Organisation, Canberra, 1999).

Shvarov, Y. (2015) A suite of programs, OptimA, OptimB, OptimC, and OptimS compatible with the Unitherm database, for deriving the thermodynamic properties of aqueous

831 species from solubility, potentiometry and spectroscopy measurements. Applied
832 Geochemistry 55, 17-27.
833 Simonson, J.M., Holmes, H.F., Busey, R.H., Mesmer, R.E., Archer, D.G. and Wood, R.H.
834 (1990) Modeling of the thermodynamics of electrolyte solutions to high temperatures
835 including ion association: application to hydrochloric acid. The Journal of Physical
836 Chemistry 94, 7675-7681.
837 Smith, D.E. and Dang, L.X. (1994) Computer simulations of NaCl association in polarizable
838 water. The Journal of Chemical Physics 100, 3757-3766.
839 Sprik, M. and Ciccotti, G. (1998) Free energy from constrained molecular dynamics. The
840 Journal of Chemical Physics 109, 7737.
841 Sprik, M. (2000) Computation of the pK of liquid water using coordination constraints.
842 Chemical Physics 258, 139-150.
843 Sretenskaya N.G. (1992) Dissociation constants of hydrochloric acid from data of electrical
844 conductance of HCl solutions in water-dioxan mixtures. Geochemistry 3, 447-453 (in
845 Russian).
846 Sulpizi, M. and Sprik, M. (2008) Acidity constants from vertical energy gaps: density
847 functional theory based molecular dynamics implementation. Physical chemistry
848 chemical physics : PCCP 10, 5238-5249.
849 Sulpizi, M. and Sprik, M. (2010) Acidity constants from DFT-based molecular dynamics
850 simulations. Journal of physics. Condensed matter : an Institute of Physics journal 22,
851 284116.
852 Sverjensky, D.A., Hemley, J.J. and D'Angelo, W.M. (1991) Thermodynamic assessment of
853 hydrothermal alkali feldspar-mica-aluminosilicate equilibria. Geochimica et
854 Cosmochimica Acta 55, 989-1004.
855 Sverjensky, D., Shock, E. and Helgeson, H. (1997) Prediction of the thermodynamic
856 properties of aqueous metal complexes to 1000 ºC and 5 kb. Geochimica et
857 Cosmochimica Acta 61, 1359-1412.
858 Sverjensky, D.A., Harrison, B. and Azzolini, D. (2014) Water in the deep Earth: The
859 dielectric constant and the solubilities of quartz and corundum to 60 kb and 1200 °C.
860 Geochimica et Cosmochimica Acta 129, 125-145.
861 Sverjensky, D.A., and Huang, F. (2015) Diamond formation due to a pH drop during fluid-
862 rock interactions. Nature Communications, 6.
863 Tagirov, B.R., Zotov, A.V. and Akinfiev, N.N. (1997) Experimental study of dissociation of
864 HCl from 350 to 500°C and from 500 to 2500 bars: Thermodynamic properties of
865 HCl°(aq). Geochimica et Cosmochimica Acta 61, 4267-4280.
866 Tremaine, P.R., Sway, K. and Barbero, J.A. (1986) The apparent molar heat capacity of
867 aqueous hydrochloric acid from 10 to 140°C. Journal of Solution Chemistry 15, 1-22.
868 Troullier, N. and Martins, J.L. (1991) Efficient pseudopotentials for plane-wave calculations.
869 Physical Review B 43, 1993-2006.
870 Trout, B.L. and Parrinello, M. (1998) The dissociation mechanism of H_2O in water studied by
871 first-principles molecular dynamics. Chemical Physics Letters 288, 343-347.
872 Zhang, Z. and Duan, Z. (2005) Prediction of the PVT properties of water over wide range of
873 temperatures and pressures from molecular dynamics simulation. Physics of the Earth
874 and Planetary Interiors 149, 335-354.
875
876

Table 1. Selected previous experimental and thermodynamic studies of the dissociation of HCl.

Method	T, P range	Log K_d (at 25 ºC)	Reference	Note
Electrical conductance	300 – 383 ºC	-	Pearson et al., 1963	Provided logK_d values at 300 – 378 ºC (ρ=0.4 – 0.7 g/cm^3)
Partial vapor pressures	25 ºC	6.18-6.31	Robinson and Bates, 1971	LogK_d were obtained from partial vapour pressure of $HCl_{(aq)}$ and LiCl solutions
Potentiometric measurement	25 ºC	0.9	Johnson and Pytkowiz, 1978	Calculated from Eq 19 in this Ref. at ionic strength = 1
Electrical conductance	100 – 700 ºC up to 4000 bar	-	Frantz et al., 1984	LogK_d in linear correlation with respect to inverse T(K) and logρ_{H2O}
Fit literature data	0 – 80 ºC	6.24	Marsh and McElory, 1985	Fitted Henry's Law constant K_h
Fit literature data	25 ºC	-	Clegg, and Brimblecombe, 1986	Refined Henry's Law constant K_h
Apparent molar heat capacity	10 – 140 ºC	-	Tremaine et al. 1986	Fitted the *Cp* value to Pitzer and HKF model
Enthalpy of dilution of $HCl_{(aq)}$	25 – 375 ºC, up to 400 bar	-	Holmes et al. (1987)	Fitted the results to Pitzer model
AgCl solubility experiment	100 – 350 ºC	0.71	Ruaya and Seward, 1987	Calculated from solubility data
Fit literature data	25 – 375 ºC, up to 400 bar	7.6[(a)] 0.2[(b)]	Simonson et al., 1990 (Eq 29 and Fig 3a in this Ref)	(a) Calculated from ion association-interaction model using Eq 29; (b) derived from chemical equilibrium model in Fig. 3a
Mineral equlibrium data for K-feldspar-muscovite-quartz	0 – 600 ºC, 500 – 2000 bar	0.86	Sverjensky et al., 1991	Experimental data at 300-600ºC, 0.5-2 kbar, and extrapolation from HKF model
Experimental data	25 ºC	0.9	Sretenskaya 1992	Electrical conductance of HCl solutions in water-dioxan mixtures
AgCl solubility experiment	300 – 500 ºC, 0.5-2 kbar	0.7	Tagirov et al 1997	Experimental data at 300-500ºC, fitting of previous data at 25-700 ºC
Volume and heat capacity	25 – 350 ºC, up to 280 bar	-	Sharygin and Wood, 1997	Fitted the C_p and V^0 values to Pitzer model
Fit literature data	0 – 1000 ºC, up to 5 kbar	6.24	Pokrovskii, 1999	Calculated from fitted HKF parameters
Conductivity Measurements	100-410ºC	-	Ho et al., 2001	Extrapolated to 600 ºC (ρ=0.4 – 0.8 g/cm^3) based on literature data
Classical MD - PMF, and review literature data	Up to 400 ºC, 700 bar	-	Chialvo et al., 2002, 2003, 2007	Rigid structural models for H_2O and H_3O^+ were applied in classical MD. Provided logK_d values as functions of density change
Ab initio MD - TI	57 ºC	7.1[(c)] 6.7[(d)]	Sulpizi and Sprik, 2008, 2010	logK_d values at 57 ºC (330K) for the studies published in (c) 2008 and (d) 2010

Abbreviations and symbols: MD = molecular dynamics; PMF = potential mean force; TI = thermodynamic integration; HKF = Helgeson-Kirkham-Flowers (Helgeson et al., 1981); Pitzer model from Pitzer, 1973; C_p = heating capacity; V^0 = molar volume; "-" means logK_d value at 25 ºC was not provided or not available in the reference.

Table 2. Details of *ab initio* MD conducted in this study. Each simulation box contains 1 HCl and 54 H_2O molecules.

T(ºC)	Box size (Å)	Density (g/cm^3)	Pressure (bar)	Simulation Time (ps)	$CN_{Cl\text{-}H}$[§]	$CN_{Cl\text{-}O}$[∞]	Chloride species*
25	11.814	0.998	1	19.16	0.00	5.89	Cl^-
100	11.956	0.963	100	15.24	0.00	5.90	Cl^-
150	12.130	0.922	100	17.42	0.00	5.82	Cl^-
200	12.358	0.871	100	17.42	0.00	5.99	Cl^-
250	12.687	0.806	100	18.54	0.01	5.52	Cl^-
300	13.192	0.717	110	16.15	0.36	4.61	Cl^-, $HCl_{(aq)}$
300	12.598	0.823	1k	15.96	0.09	5.39	Cl^-
300	11.826	0.995	5k	15.96	0.00	6.82	Cl^-
350	13.993	0.600	200	16.62	0.94	2.95	$HCl_{(aq)}$
400	16.187	0.388	308	17.20	1.00	1.70	$HCl_{(aq)}$
400	13.342	0.693	1k	18.00	0.97	3.74	$HCl_{(aq)}$
400	12.083	0.933	5k	18.14	0.10	6.33	Cl^-
500	13.772	0.630	1.5k	18.28	0.98	3.27	$HCl_{(aq)}$
600	13.651	0.647	2.5k	18.25	0.99	3.61	$HCl_{(aq)}$
700	13.574	0.658	3.5k	15.18	1.00	3.68	$HCl_{(aq)}$
700	12.156	0.916	10k	16.69	0.63	5.98	$HCl_{(aq)}$, Cl^-
700	11.454	1.095	20k	17.42	0.16	8.03	Cl^-, $HCl_{(aq)}$
700	10.504	1.420	60k	21.04	0.02	11.4	Cl^-

¶ Density of 55 H_2O in the cubic box. Water density data of pressure up to 10 kbar are from NIST (Lemmon et al., 2000), and above 10 kbar are from Zhang and Duan (2005).

§ Cl-H distance cutoff at 1.6 Å

∞Cl-O distance cutoff at 3.8 Å

*Chloride species with > 10% of the total population is listed.

Table 3. Gibbs free energy for reaction (1) and Gibbs free energy of formation from the elements for $HCl_{(aq)}$ from the MD simulations.

T (˚C)	P (bar)	$\Delta_r G_r(P,T)$ (kJ/mol) ¶	$\Delta G_r^0(P_r,T_r)$ $\Delta_r G^{\Theta}(P_r,T_r)$ (kJ/mol) ¶	$\Delta G_{f,Cl^-}^0$ (kJ/mol)#	$\Delta G_{f,HCl_{(aq)}}^0$ (kJ/mol)	logK§ (MD)	logK$^{\infty}$ (HKF)
25	1	-39.72±3.60	-38.90±3.60	-131.29	-92.39	6.81±0.63	6.81
100	100	-40.42±5.21	-39.23±5.21	-134.42	-95.19	5.49±0.73	4.56
150	100	-34.00±5.91	-32.36±5.91	-135.66	-103.30	3.99±0.73	3.27
200	100	-27.77±6.47	-25.49±6.47	-136.01	-110.52	2.81±0.71	2.09
250	100	-17.78±3.84	-14.61±3.84	-135.12	-120.51	1.46±0.38	0.93
300	110	6.58±1.33	11.04±1.33	-132.03	-143.07	-1.01±0.12	-0.33
300	1k	-12.04±3.54	-8.24±3.54	-134.75	-126.51	0.75±0.32	0.69
300	5k	-30.28±4.19	-28.15±4.19	-132.15	-104.00	2.57±0.38	2.37
350	200	23.90±1.75	30.41±1.75	-124.98	-155.39	-2.55±0.15	-1.89
400	308	48.25±1.70	58.31±1.70	-111.07	-169.38	-4.52±0.13	-4.80
400	1k	9.58±1.11	16.52±1.11	-130.07	-146.59	-1.28±0.09	-1.29
400	5k	-11.95±5.35	-8.65±5.35	-133.39	-124.74	0.67±0.42	0.98
500	1.5k	36.38±2.12	46.31±2.12	-124.94	-171.25	-3.13±0.14	-2.58
600	2.5k	35.01±4.69	45.16±4.69	-124.08	-169.24	-2.70±0.28	-2.95
700	3.5k	47.47±3.57	58.79±3.57	-123.04	-181.83	-3.16±0.19	-3.30
700	10k	8.88±4.91	16.87±4.91	-128.33	-145.20	-0.91±0.26	-1.09
700	20k	-14.89±5.97	-7.77±5.97	-119.00	-111.23	0.42±0.32	0.36
700	60k	-49.72±4.88	-46.27±4.88	-57.91	-11.64	2.48±0.26	3.06

$\Delta G_{f,j}^0$ refers to standard partial molal Gibbs free energy of formation of the species *j* from its elements in their stable state at the reference temperature and pressure (25 ºC, 1 bar); $\Delta G_{f,Cl^-}^0$ values up to 5 kbar were calculated from HCh (Shvarov and Bastrakov, 1999; Shvarov, 2008) using HKF parameters from Shock and Helgeson (1988), at 700 ºC, 60 kbar the value was calculated from DEW model (Sverjensky et al., 2014) using the same HKF parameters.

¶ $\Delta G_r(P,T)$ is the Gibbs free energy of Eq (1) calculated from thermodynamic integration and $\Delta G_r^0(P_r,T_r)$ is the standard state Gibbs free energy at infinite dilution calculated using the B-dot activity model.

LogK_d calculated from: §MD simulations using Eq (4); $^{\infty}$HCh (Shvarov and Bastrakov, 1999; Shvarov, 2008) using fitted HKF parameters (Table 4) for pressure up to 5 kbar, and DEW model (Sverjensky et al., 2014) using fitted HKF parameters for pressure above 5 kbar.

Table 4. Equation-of-state parameters and standard partial molal properties (HKF parameters) for HCl(aq) regressed from logK data from MD simulations in this study (as listed in Table 3).

Parameters	$HCl_{(aq)}$
$\Delta_f \overline{G}^0_{P_r,T_r}$ (cal mol^{-1})	-22091
$\overline{S}^0_{P_r,T_r}$ (cal mol^{-1} K^{-1})	28.744
a_1 (cal mol^{-1} bar^{-1})×10	6.9732
a_2 (cal mol^{-1})×10^{-2}	41.9381
a_3 (cal mol^{-1} bar^{-1})	-119.8177
a_4 (cal mol^{-1})×10^{-4}	-4.5127
c_1 (cal mol^{-1})	5.9112
c_2 (cal K mol^{-1}) ×10^{-4}	11.8269
W_{P_r,T_r} (cal mol^{-1}) ×10^{-5}	-0.6291

Table 5. Logarithm of the dissociation constants for $HCl_{(aq)}$ ($\log K_d$) calculated using HCh (Shvarov and Bastrakov, 1999; Shvarov, 2008) based on fitted HKF parameters as listed in Table 4.

T(°C)	Pressure (bar)						
	P_{sat}	100	300	500	1k	2k	5k
25	6.81	6.80	6.79	6.76	6.63	6.22	4.33
50	5.98	6.02	6.07	6.11	6.16	6.13	5.38
100	4.50	4.56	4.67	4.77	4.97	5.23	5.46
150	3.20	3.27	3.40	3.53	3.79	4.18	4.79
200	2.01	2.09	2.24	2.39	2.69	3.16	3.97
250	0.86	0.93	1.13	1.31	1.67	2.20	3.15
300	-0.38	-0.35	-0.02	0.23	0.69	1.31	2.37
350	-2.14	gas	-1.47	-0.96	-0.28	0.46	1.65
400	---	gas	-5.42	-2.37	-1.29	-0.36	0.98
450	---	gas	gas	-5.19	-2.41	-1.16	0.35
500	---	gas	gas	gas	-3.73	-1.96	-0.25
550	---	gas	gas	gas	-5.29	-2.77	-0.81
600	---	gas	gas	gas	-6.95	-3.59	-1.35
650	---	gas	gas	gas	-8.49	-4.40	-1.88
700	---	gas	gas	gas	gas	-5.20	-2.39

Table 6. Logarithm of the dissociation constants for $HCl_{(aq)}$ ($\log K_d$) calculated using the DEW model (Sverjensky et al., 2014) based on the fitted HKF parameters listed in Table 4.

T(°C)	Pressure (kbar)						
	10	20	30	40	50	60	70
300	3.31	4.18	4.61	4.83	4.95	5.00	5.00
350	2.68	3.70	4.28	4.67	4.95	5.16	5.33
400	2.06	3.19	3.87	4.36	4.75	5.08	5.36
450	1.47	2.68	3.43	3.99	4.45	4.85	5.20
500	0.91	2.18	2.98	3.59	4.10	4.55	4.95
550	0.38	1.70	2.53	3.18	3.72	4.20	4.63
600	-0.13	1.23	2.09	2.76	3.32	3.83	4.29
650	-0.62	0.79	1.67	2.35	2.93	3.45	3.92
700	-1.09	0.36	1.25	1.95	2.54	3.06	3.55
750	-1.55	-0.05	0.85	1.56	2.15	2.69	3.18
800	-1.99	-0.45	0.47	1.18	1.78	2.31	2.81
850	-2.41	-0.83	0.10	0.81	1.41	1.95	2.44
900	-2.83	-1.20	-0.27	0.45	1.05	1.59	2.09
950	-3.23	-1.56	-0.61	0.10	0.71	1.24	1.74
1000	-3.62	-1.91	-0.95	-0.24	0.37	0.90	1.40

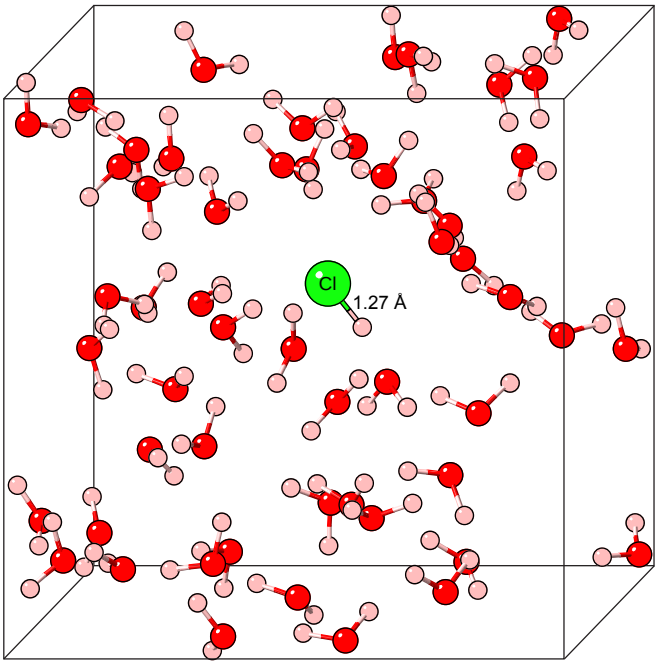

Fig. 1. Simulation set up for HCl in aqueous solution (green: chlorine; red: oxygen; pink: hydrogen).

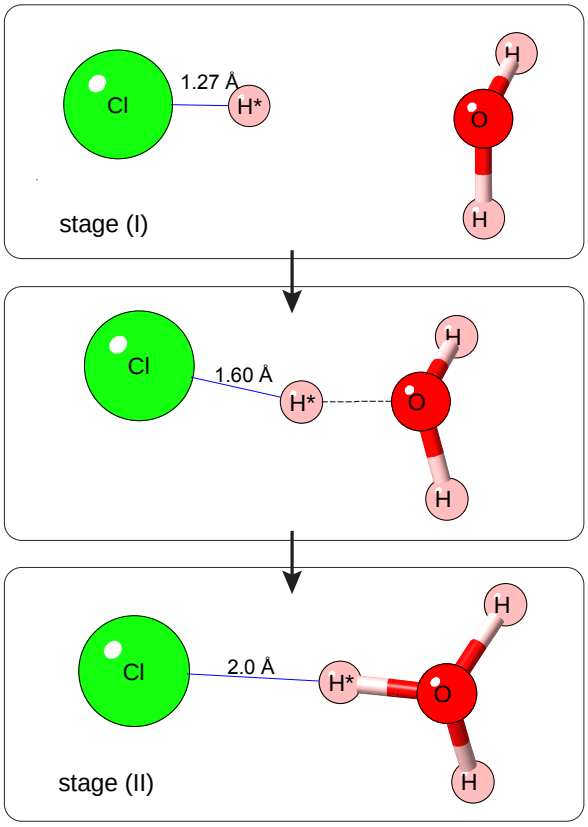

Fig. 2. Reaction paths and constrained bond distances for dissociation reaction of $HCl_{(aq)}$. The hydration shell of Cl is not shown.

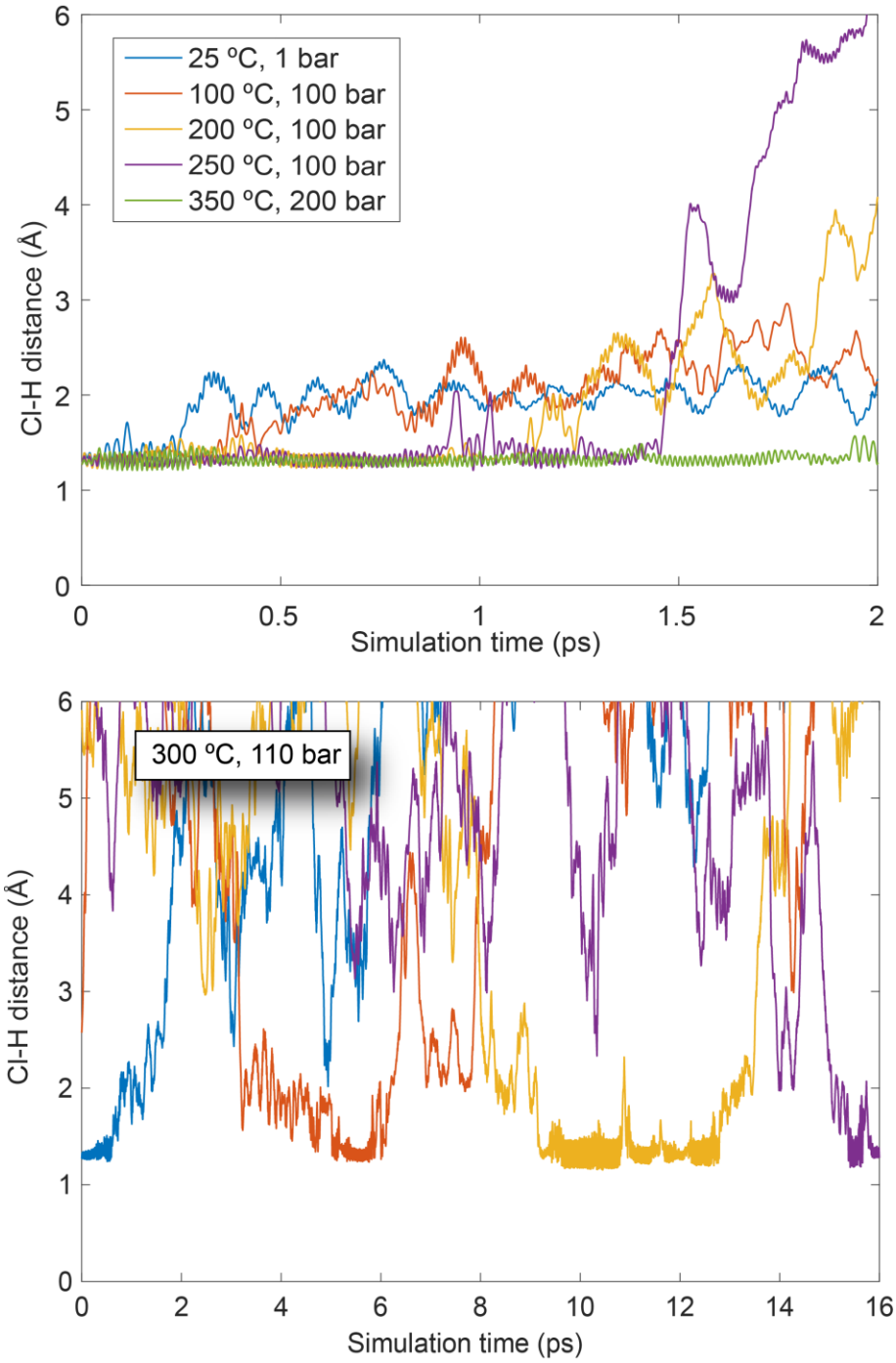

Fig. 3. (a) H-Cl distances as a function of time show the extent of dissociation of $HCl_{(aq)}$ molecule in aqueous solution at different temperatures and pressures; (b) distance between Cl and four selected H atoms shows the dissociation-association of $HCl_{(aq)}$ in aqueous solution at 300 ºC, 110 bar.

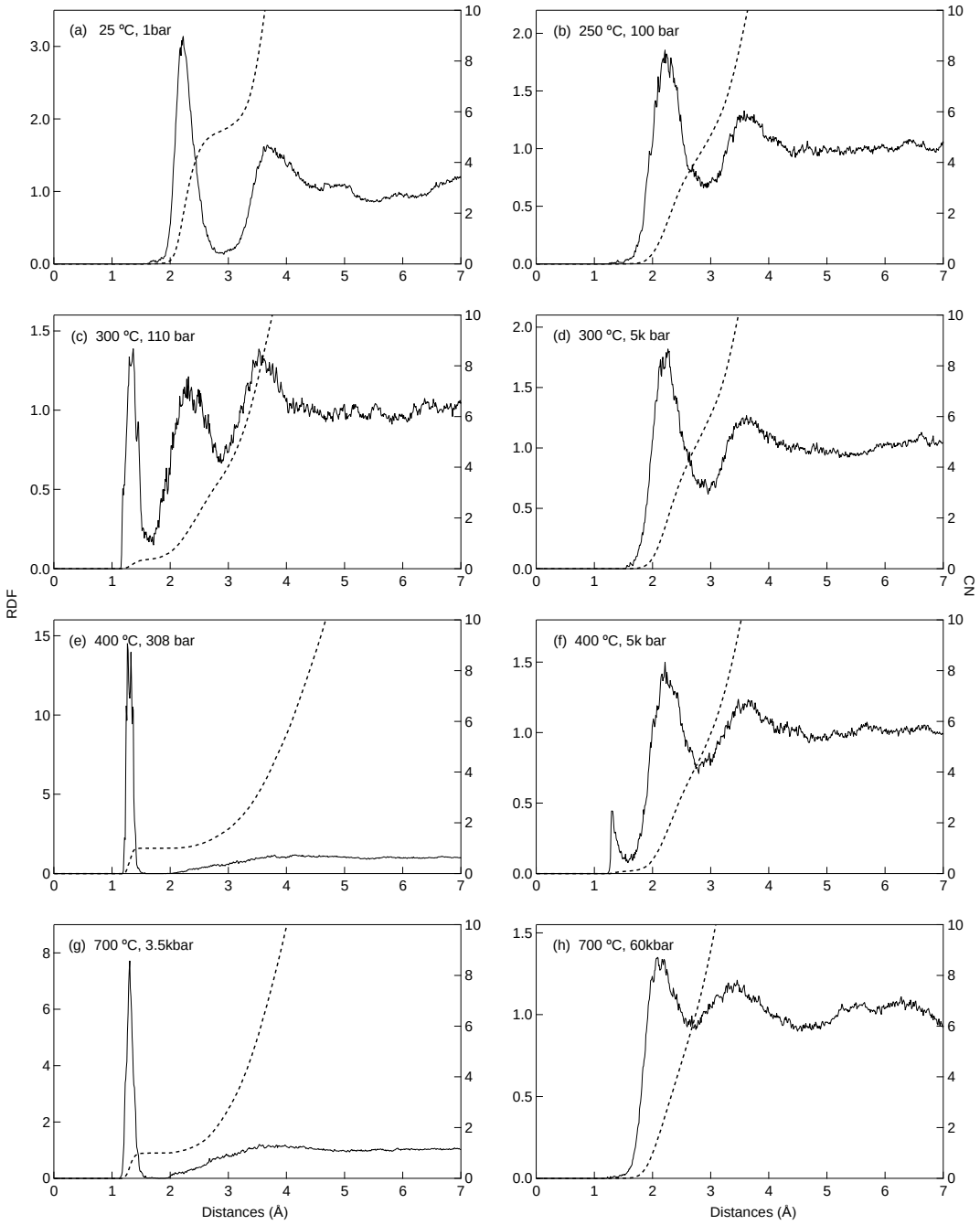

Fig. 4. Radial distribution functions (RDF, left Y-axes, solid lines) of Cl-H and their integrals (coordination number (CN), right Y-axes, dashed lines) at 25 – 700 ºC, at various pressures, calculated after 1.4 ps of equilibration.

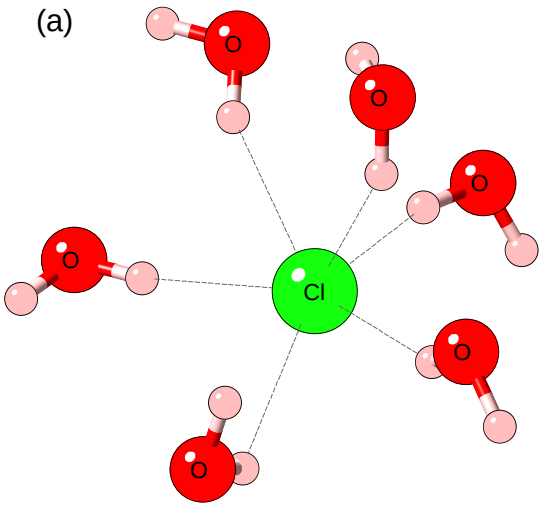

a snapshot of $Cl(H_2O)_6^-$ at 25 ºC, 1 bar

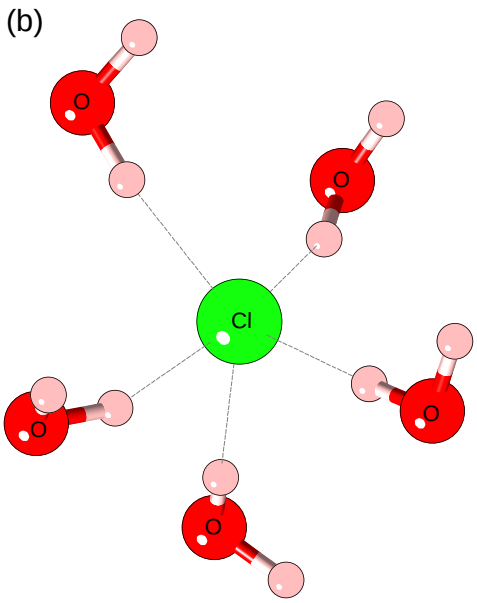

a snapshot of $Cl(H_2O)_5^-$ at 300 ºC, 110 bar

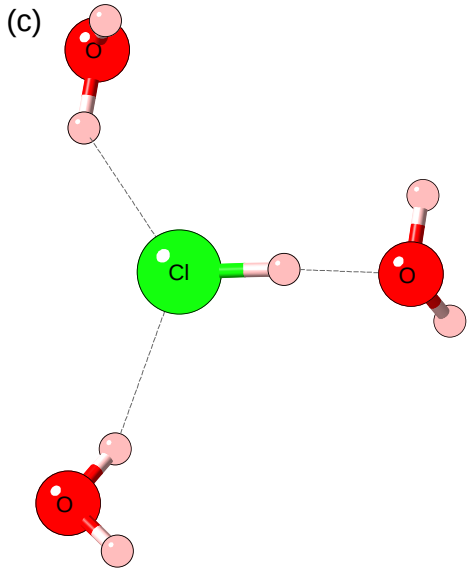

a snapshot of $HCl(H_2O)_3$ at 300 ºC, 110 bar

Fig. 5. Snapshots of the first hydration shell of chloride for simulations at 25 ºC, 1 bar (a), and 300 ºC, 110 bar (b,c).

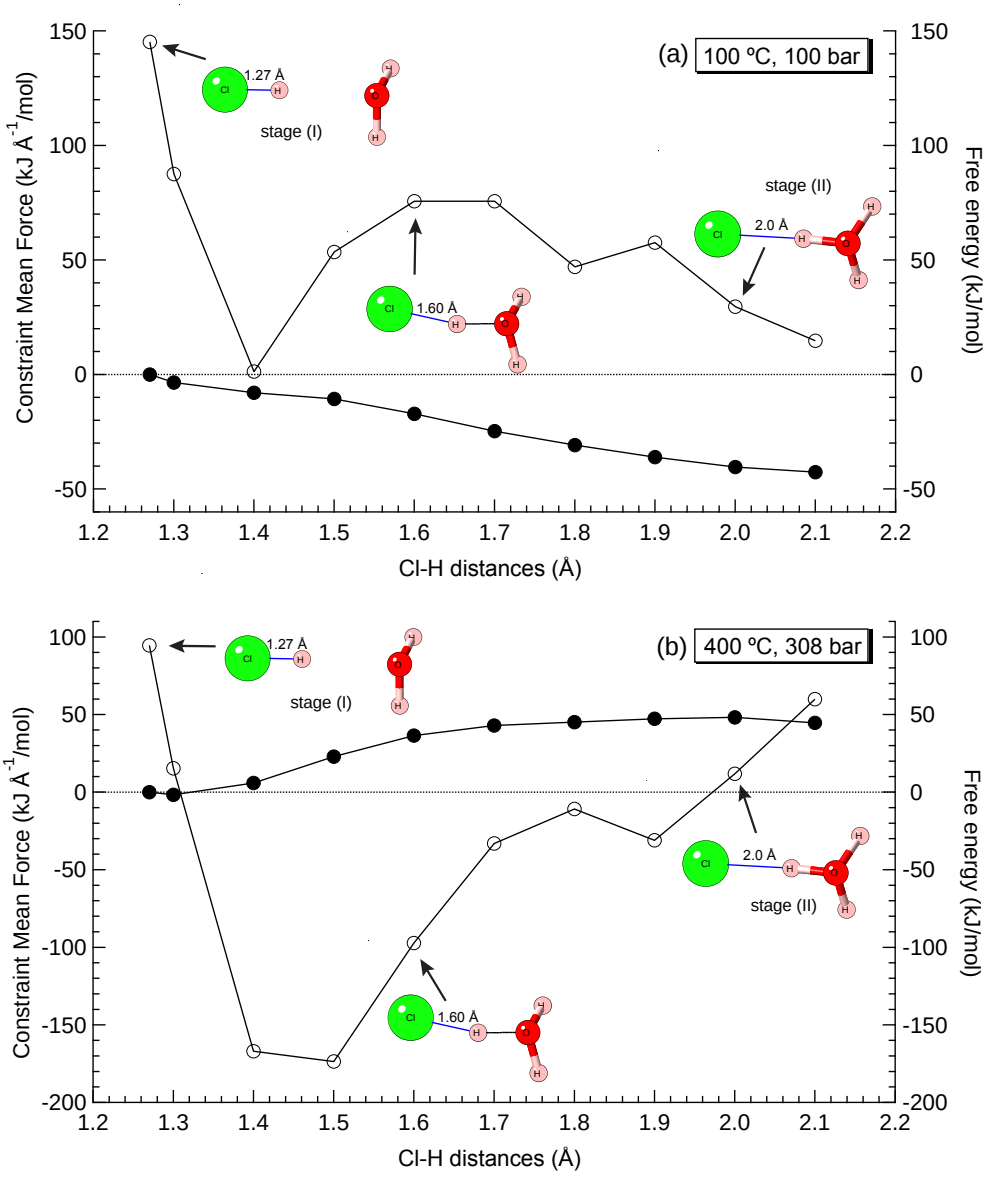

Fig. 6. Examples of constrained mean forces (empty circles) and their integrated values (solid circles), which correspond to the free energy, for the reaction $HCl_{(aq)} + H_2O = Cl^- + H_3O^+$ at (a) 100 ºC, 100 bar, and (b) 400 ºC, 308 bar. The empty circles are the running averages of constraint forces at each distance, and the solid circles are the numerical integrals of the mean constraint force with respect to the distance.

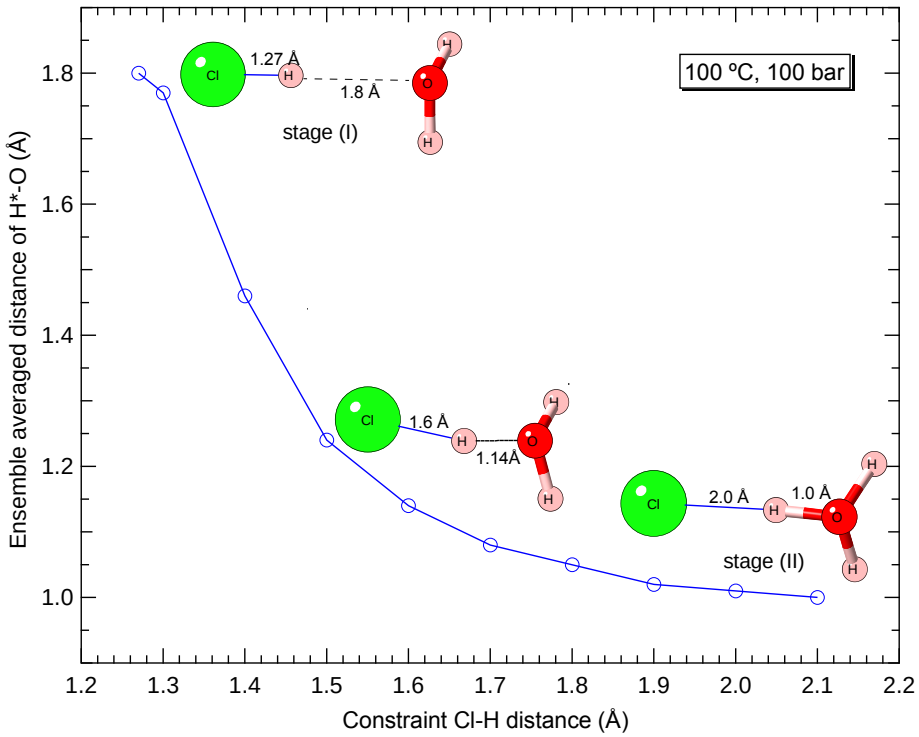

Fig. 7. Distances of H*-O as a function of the constraint Cl-H coordinate at 100 ºC, 100 bar for the $HCl_{(aq)}$ dissociation reaction (Eq. 3).

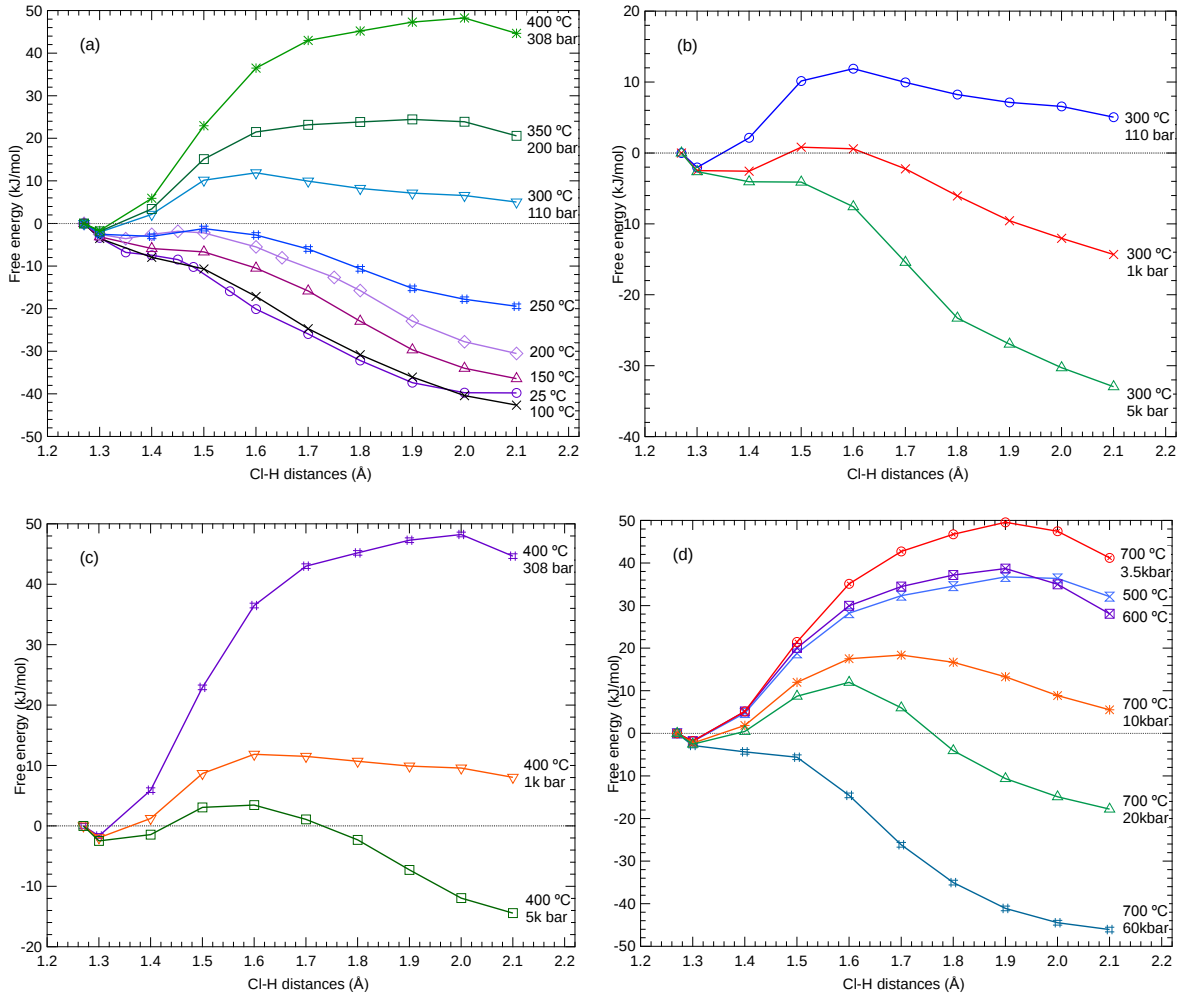

Fig. 8. Free energy surface of $HCl_{(aq)}$ dissociation reaction at (a) 25 – 400 ºC, Psat – 308 bar; (b) 300 ºC, 110 – 5 kbar; (c) 400 ºC, 308 – 5 kbar; (d) 500 – 700 ºC, 1.5k – 60 kbar. The free energy values of the reactions at each T-P conditions were chosen at the Cl-H distance of 2.0 Å.

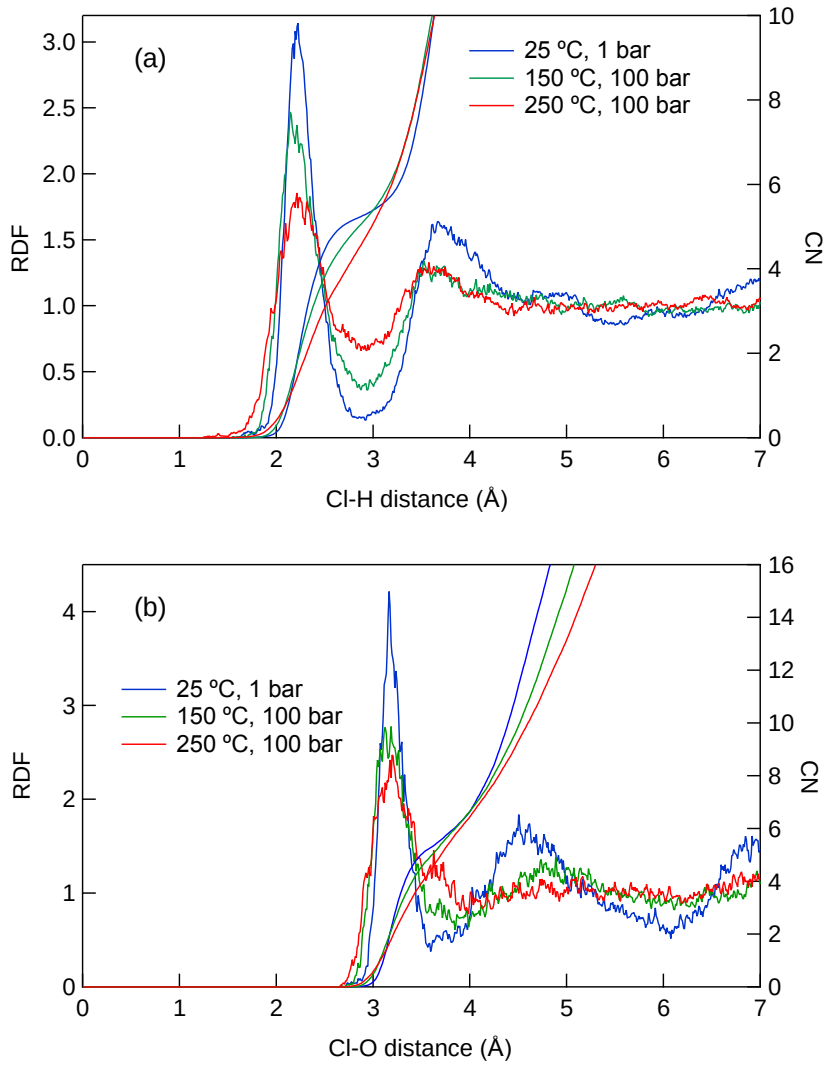

Fig. 9. RDF plot of (a) Cl-H and (b) Cl-O at 25 ºC, 1 bar (0.998 g/cm^3), 150 ºC, 100 bar (0.922 g/cm^3) and 250 ºC, 100 bar (0.806 g/cm^3) to show (a) the change of H-bond; (b) the change of Cl^- hydration as function of temperature.

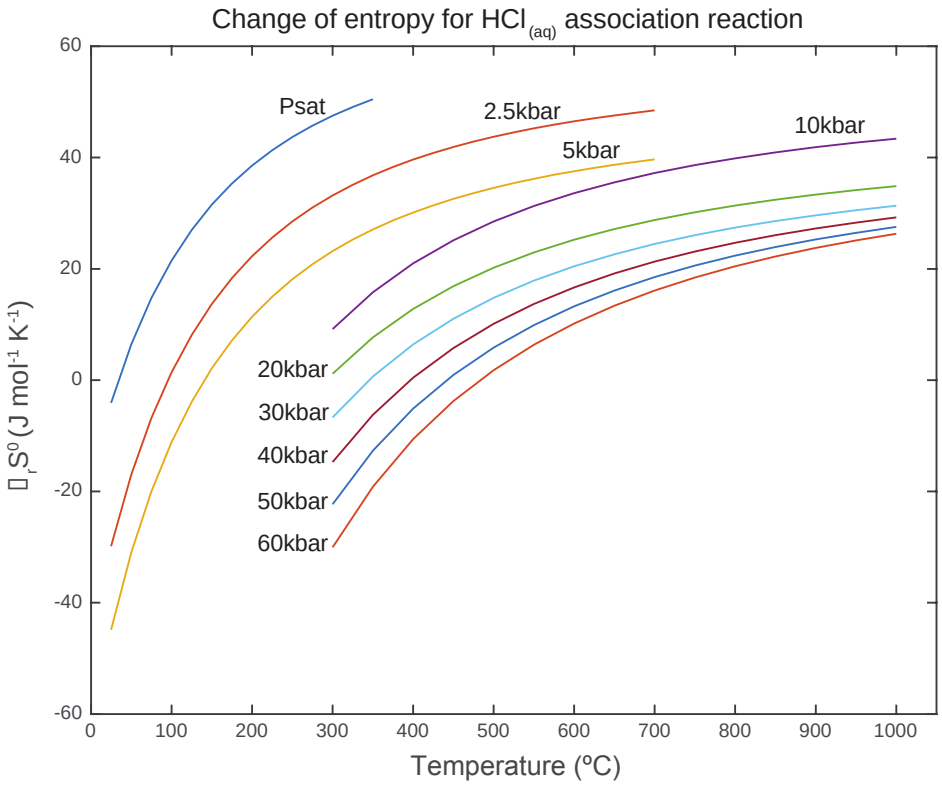

Figure 10. Change of entropy for $HCl_{(aq)}$ association reaction ($H^+ + Cl^- = HCl_{(aq)}$) at different T-P. The change of entropy $\Delta_r S^0$ is calculated from $\Delta S = R' (a - \frac{c}{T^2})$, where R is the gas constant, a and c are the parameters fitted from $\ln K_{eq} = a + \frac{b}{T} + \frac{c}{T^2}$ (Galaon and David, 2011).

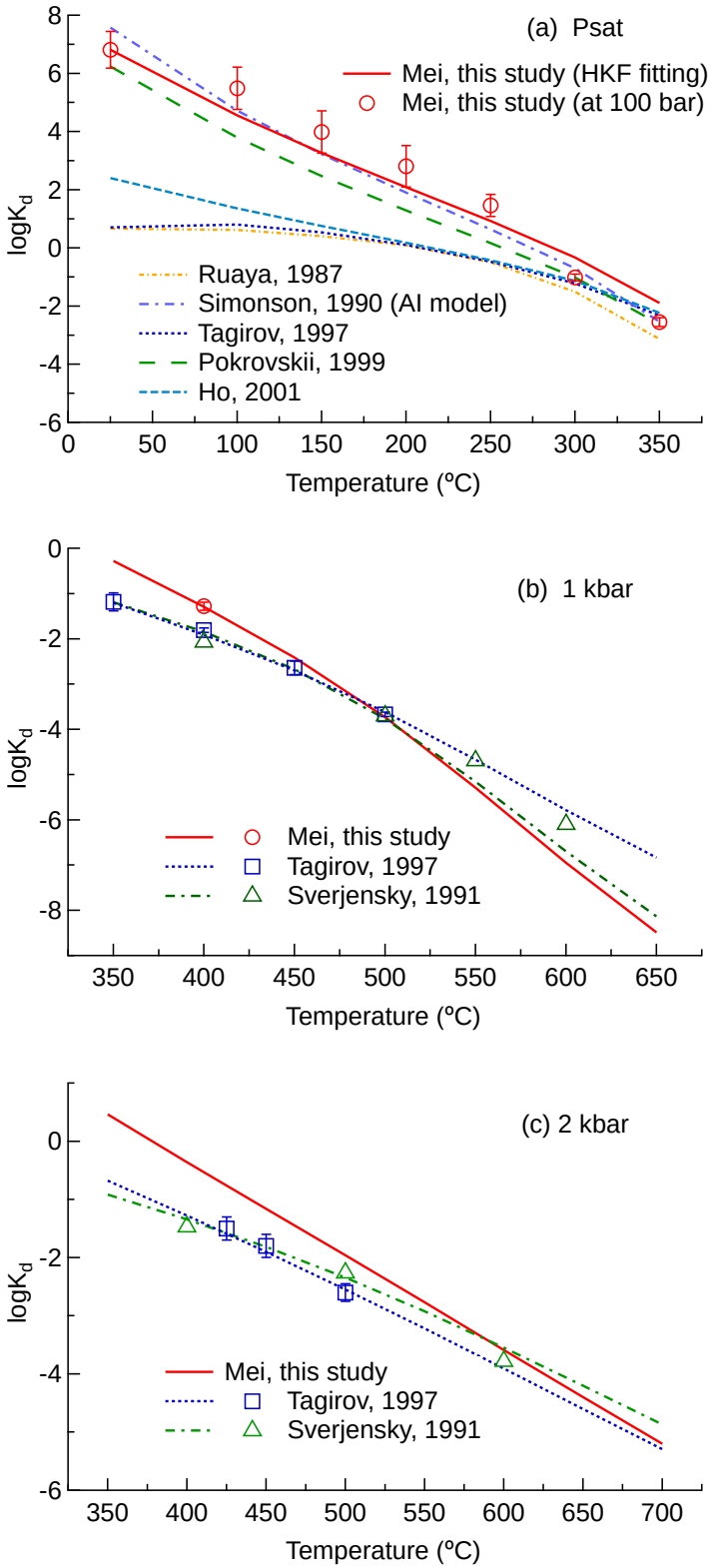

Fig. 11. LogK_d values of $HCl_{(aq)}$ as function of temperature (a) at 25 – 350 ºC, P_{sat}, (b) 350 – 650 ºC, 1 kbar and (c) 350-700 ºC, 2 kbar. The solid and dash lines show logK_d calculated based on the HKF parameters from different studies as noted; the circles, squares and triangles with error bars show the direct logK_d values from experiments and MD simulations.

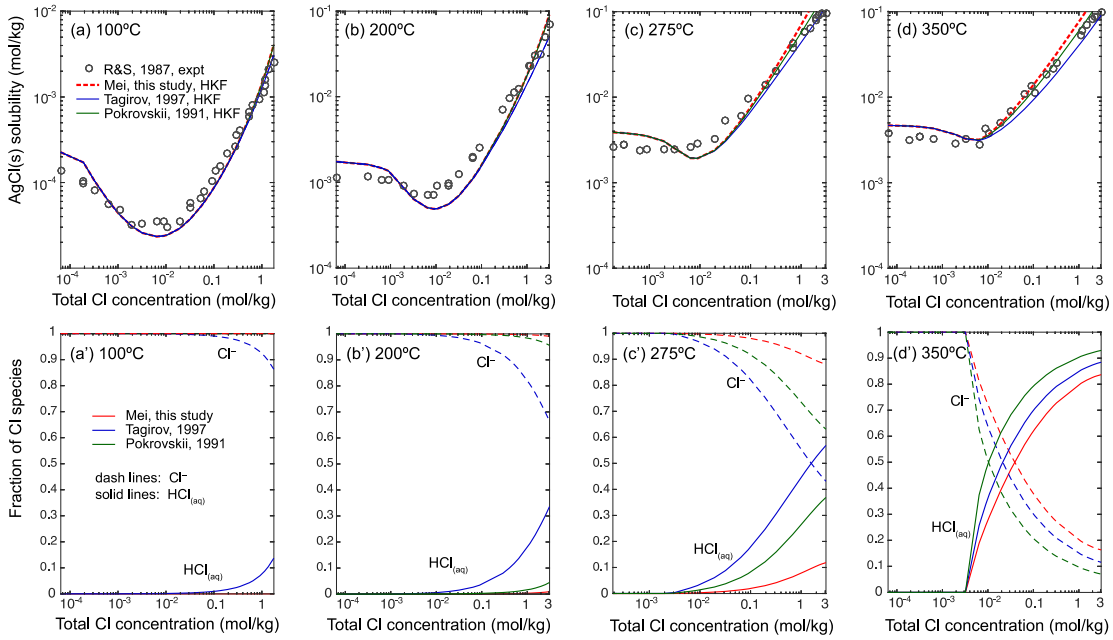

Figure 12. (a-d) Solubility of AgCl from experiment data by Ruaya and Seward (1987) (grey circles) and calculated values using $HCl_{(aq)}$ HKF paramters from Tagirov et al. (1997), Pokrovskii (1999) and this study; (a'-d') the fraction of Cl species at calculated temperature using HKF parameters from Tagirov et al. (1997), Pokrovskii (1999) and this study.

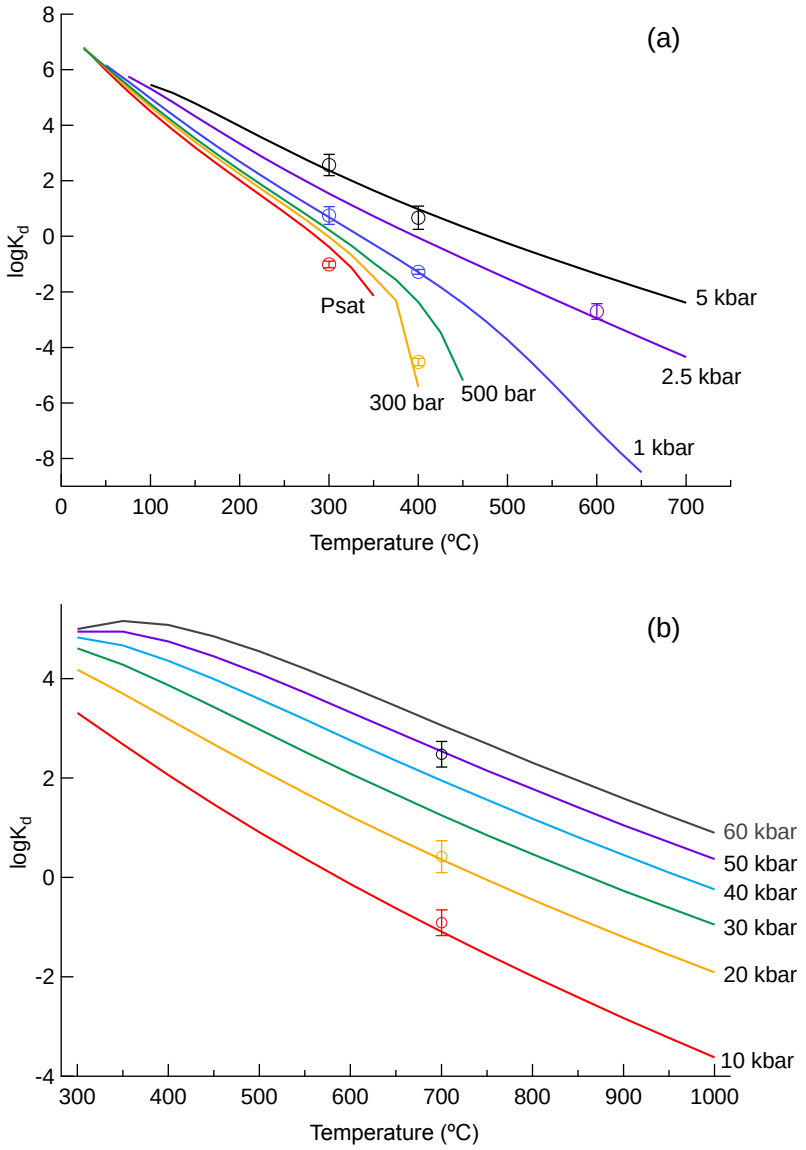

Figure 13. LogK_d extrapolated using HKF parameters listed in Table 4 from fitting of MD values (a) 25-700ºC, Psat-5 kbar, and (b) extrapolation to high pressure (10-60kbar) using the DEW model (Sverjensky et al., 2014). The circles with error bars show the logK_d values directly calculated from MD calculation (as listed in Table 3) at a given pressure as indicated by the different colors.